NASA CR-135349
PSI TR-97

ANALYTICAL STUDY OF LASER SUPPORTED COMBUSTION WAVES IN HYDROGEN

by

N. H. Kemp and R. G. Root

PHYSICAL SCIENCES INC.

prepared for

NATIONAL AERONAUTICS AND SPACE ADMINISTRATION
LEWIS RESEARCH CENTER

Contract NAS 3-20381

August 1977

1. Report No.	2. Government Accession No.	3. Recipient's Catalog No.
NASA CR-135349		

4. Title and Subtitle	5. Report Date
ANALYTICAL STUDY OF LASER SUPPORTED COMBUSTION WAVES IN HYDROGEN	August 1977
	6. Performing Organization Code: 6K561

7. Author(s)	8. Performing Organization Report No.
N. H. Kemp and R. G. Root	PSI TR-97

9. Performing Organization Name and Address	10. Work Unit No.
Physical Sciences Inc. 30 Commerce Way Woburn, MA 01801	Y0V6858
	11. Contract or Grant No.: NAS 3-20381

12. Sponsoring Agency Name and Address	13. Type of Report and Period Covered
National Aeronautics and SpaceAdministration Lewis Research Center Cleveland, OH 44135	Final Report 10/12/76 - 4/12/77
	14. Sponsoring Agency Code

15. Supplementary Notes

Project Monitor, Stephen M. Cohen, Laser and Energy Systems Branch, NASA Lewis Research Center, Cleveland, Ohio

16. Abstract

Reference 1 describes a study of a CW laser-heated hydrogen rocket using 10.6 μm radiation. It was found that the properties of Laser Supported Combustion (LSC) waves in hydrogen were an important ingredient in modeling this rocket. They determine the temperature level reached by the gas, and the mass flux through the rocket. No theoretical or experimental studies of LSC waves in hydrogen were available. Therefore, a theoretical study of such waves has been made. A one-dimensional energy equation, with constant pressure and area, was used to model the LSC wave. This equation balances convection, conduction, laser energy absorption, radiation energy loss and radiation energy transport. The latter is shown to be approximated well by a radiation conduction model. Solutions of this energy equation were obtained to give profiles of temperature and other properties, as well as the relation between laser intensity and mass flux through the wave. The calculations cover the pressures of 1, 3, 10 and 30 atm, 10.6 μm laser intensities from 10^4 W/cm^2 to 10^6 W/cm^2 and power levels of 10 kW and 5 MW. The physics of these waves leads to high peak temperatures (on the order of 20,000 K), because the absorption mechanism is inverse bremsstrahlung, which requires a significant degree of ionization, and this occurs in hydrogen only above about 10,000 K. The high temperatures also lead to considerable radiation losses.

The flow through the LSC wave was then conducted through a variable-pressure, variable-area streamtube to accelerate it to high speed, with the propulsion application in mind. A numerical method for coupling the LSC wave model to the streamtube flow was developed, and a sample calculation was performed. The result shows that 42% of the laser power has been radiated away by the time the gas reaches the throat. This is in contrast with results for a similar case calculated in Ref. 1, where the LSC wave properties were only estimated, not calculated. There only 5% of the power was found to be lost. The present more realistic

(over)

17. Key Words (Suggested by Author(s))	18. Distribution Statement
Laser Propulsion Hydrogen Plasma Radiation Hydrogen Nozzle Flow LSC Waves	Unlimited

19. Security Classif. (of this report)	20. Security Classif. (of this page)	21. No. of Pages	22. Price*
Unclassified	Unclassified	118	

* For sale by the National Technical Information Service, Springfield, Virginia 22161

calculations show the large losses incurred by the necessity of operating at high temperatures in hydrogen.

Several two-dimensional effects were estimated. Radial losses due to heat conduction and black radiation from the edge of the hot gas were found important at the 10 kW power level. They cause the intensity threshold for existence of the LSC wave to the rise to values considerably higher than that which prevails if these losses are ignored. Beam convergence effects were also estimated by including beam area change in the laser absorption term. A calculation showed the mass flux required in a converging beam to be larger than in a parallel beam of the same initial intensity. Converging beams provide static stability for the wave position. Transverse velocity was also considered. It was concluded that in the radially confined flows of interest for propulsion applications, transverse velocities would be less important than in the unconfined flows where air experiments have been conducted.

It would be advantageous to produce LSC waves at lower temperatures to reduce the large radiation losses. This can be accomplished by introducing easily ionized seed into the hydrogen to allow laser absorption at lower temperatures. The amount of seed must be small enough so that the specific impulse is not adversely affected by its weight. It is recommended that studies of LSC waves in seeded hydrogen be conducted.

NASA CR-135349

PSI TR-97

ANALYTICAL STUDY OF LASER SUPPORTED COMBUSTION WAVES IN HYDROGEN

by

N. H. Kemp and R. G. Root

PHYSICAL SCIENCES INC.
30 Commerce Way
Woburn, MA 01801

prepared for

NATIONAL AERONAUTICS AND SPACE ADMINISTRATION
LEWIS RESEARCH CENTER

Contract NAS 3-20381

August 1977

FOREWORD

The research described in this report was performed for the Laser Systems Section at the NASA/Lewis Research Center under Contract NAS3-20381. The NASA Project Manager was Mr. Stephen M. Cohen.

The beam shape used in Subsection 4.2 was suggested by Dr. Peter Nebolsine. Efficient computational assistance was provided by Edward Tomaszewski.

SUMMARY

Reference 1 describes a study of a CW laser-heated hydrogen rocket using 10.6 μm radiation. It was found that the properties of Laser Supported Combustion (LSC) waves in hydrogen were an important ingredient in modeling this rocket. They determine the temperature level reached by the gas, and the mass flux through the rocket. No theoretical or experimental studies of LSC waves in hydrogen were available. Therefore, a theoretical study of such waves has been made. A one-dimensional energy equation, with constant pressure and area, was used to model the LSC wave. This equation balances convection, conduction, laser energy absorption, radiation energy loss and radiation energy transport. The latter is shown to be approximated well by a radiation conduction model. Solutions of this energy equation were obtained to give profiles of temperature and other properties, as well as the relation between laser intensity and mass flux through the wave. The calculations cover the pressures of 1, 3, 10 and 30 atm, 10.6 μm laser intensities from 10^4 W/cm^2 to 10^6 W/cm^2 and power levels of 10 kW and 5 MW. The physics of these waves leads to high peak temperatures (on the order of 20,000K), because the absorption mechanism is inverse bremsstrahlung, which requires a significant degree of ionization, and this occurs in hydrogen only above about 10,000K. The high temperatures also lead to considerable radiation losses.

The flow through the LSC wave was then conducted through a variable-pressure, variable-area streamtube to accelerate it to high speed, with the propulsion application in mind. A numerical method for coupling the LSC wave model to the streamtube flow was developed, and a sample calculation was performed. The result shows that 42% of the laser power has been radiated away by the time the gas reaches the throat. This is in contrast with results for a similar case calculated in Ref. 1, where the LSC wave properties were only

estimated, not calculated. There only 5% of the power was found to be lost. The present more realistic calculations show the large losses incurred by the necessity of operating at high temperatures in hydrogen.

Several two-dimensional effects were estimated. Radial losses due to heat conduction and black radiation from the edge of the hot gas were found important at the 10 kW power level. They cause the intensity threshold for existence of the LSC wave to rise to values considerably higher than that which prevails if these losses are ignored. Beam convergence effects were also estimated by including beam area change in the laser absorption term. A calculation showed the mass flux required in a converging beam to be larger than in a parallel beam of the same initial intensity. Converging beams provide static stability for the wave position. Transverse velocity was also considered. It was concluded that in the radially confined flows of interest for propulsion applications, transverse velocities would be less important than in the unconfined flows where air experiments have been conducted.

It would be advantageous to produce LSC waves at lower temperatures to reduce the large radiation losses. This can be accomplished by introducing easily ionized seed into the hydrogen to allow laser absorption at lower temperatures. The amount of seed must be small enough so that the specific impulse is not adversely affected by its weight. It is recommended that studies of LSC waves in seeded hydrogen be conducted.

TABLE OF CONTENTS

LIST OF ILLUSTRATIONS

LIST OF ILLUSTRATIONS (Cont'd)

LIST OF TABLES

1. INTRODUCTION

In a recent study of CW laser propulsion, Ref. 1, an analysis was made of the specific impulse which could be obtained by heating hydrogen with a 10.6 μm laser beam. With this combination of gas and laser frequency, the only mechanism by which the laser energy can be absorbed in the gas is inverse bremsstrahlung. This mechanism requires the presence of electrons and therefore will only become operable when the hydrogen ionizes at temperatures of 10,000K or more. Other phenomena must operate to heat the gas from ambient temperature to these high temperatures.

It has been known for some time that a mechanism to achieve this heating exists for air, known as a laser-supported combustion (LSC) wave. This wave is analogous to a deflagration wave in ordinary chemical combustion, but the energy source is a laser beam, rather than chemical energy. The LSC wave consists of an approximately constant pressure region in which the gas temperature rises sharply to a high value, and then decays slowly. The high temperature region is maintained by the absorption of the laser energy by the gas. The rapid temperature rise is produced by the transport of energy from the hot region into the cold gas by both thermal conduction and radiation. The decay of the temperature at the back of the wave is caused by radiation losses dominating the absorption of laser energy, because the energy in the laser beam has already been almost completely absorbed by the gas in the hot region.

The energy transport by conduction and radiation in an LSC wave therefore provides a mechanism to heat cold gas up to a temperature where laser energy can be absorbed by a high temperature mechanism like inverse bremsstrahlung. Such waves have been observed in air and the rare gases, though there are no reports of any attempt to generate them in hydrogen.

The laser-heated hydrogen rocket is thus envisioned to have an LSC wave standing at the front of the heating region. Cold hydrogen flows in, is heated and absorbs laser energy at high temperatures. It is then expanded through a nozzle to a high velocity to impart thrust to the rocket.

Raizer (Ref. 2) was the first to recognize the possibility of such a wave, though he considered primarily thermal conduction, not radiation, as the forward energy transport mechanism.

Boni and Su (Ref. 3) and Jackson and Nielsen (Ref. 4) added the effect of radiation, which they found to be important in many cases. Additional modeling for air has been done Boni and Su (Refs. 5 and 6) and by others. Recently Pirri et al (Ref. 7) have improved the radiation model in an air LSC wave, and developed a simple numerical calculation scheme for computing the temperature profile.

Experimental observations of LSC waves in air have been made by Klosterman and Byron (Ref. 8) among others, and in rare gases by Soviet investigators, but not in hydrogen.

An important feature of these waves is their speed. The models indicate that the speed of an LSC wave in a given gas is a unique function of the laser intensity. Since the wave in the laser-heated rocket is to be stationary, it is important to know the relationship between speed and intensity, so the proper inflow velocity of the hydrogen to hold the wave fixed may be chosen for the intensity used.

This inflow determines the mass flow per unit area in the rocket, and so affects the thrust level which can be achieved for a given cross-sectional area. Therefore, thrust and power scale linearly with area.

In the study of Ref. 1 it was noted that in the absence of either models or experiments for hydrogen, an estimate would have to be made of wave speed versus intensity. Such an estimate was made, using the method of Ref. 4 and a crude approximation to the radiation

properties of hydrogen. However, the uncertainty in the resulting speed was felt to be considerable. Since this parameter is so important to the design of a laser-heated hydrogen rocket, and since experiments on LSC waves and rockets are underway at NASA Lewis Research Center, it seems desirable to develop a model of LSC waves in hydrogen. The work reported here describes such a model, based on the comparatively simple numerical methods of Ref. 7, and detailed consideration of the thermodynamic and radiation properties of hydrogen.

In Section 2, a one-dimensional model of the hydrogen LSC wave is developed by solving the energy conservation equation, including convection, laser absorption, radiation losses to the environment, radiation transport of energy from one part of the wave to another, and thermal conduction. Calculations are made for laser intensities from 10^4 to 10^6 W/cm^2, at pressures of 1, 3, 10 and 30 atm, for laser powers of 10 kW and 5 MW. The resulting wave speed, mass flow and temperature parameters are tabulated for 45 cases.

In Section 3, the acceleration of the gas coming out of the LSC wave by a variable area, variable pressure channel is considered. This represents the nozzle necessary to accelerate the gas to produce thrust. The purpose of this section is to develop a computational method for coupling the LSC wave model to the nozzle flow. One case is computed to demonstrate the use of the proposed method of coupling for a specific set of parameters.

Section 4 is concerned with two-dimensional effects which may be of importance to the wave speed. We consider radial heat losses due to conduction and black radiation emission from the edges of the hot gas cylinder; convergence of the laser beam; and transverse flow velocities.

Section 5 sets forth the conclusions which can be drawn, and how they affect the results of Ref. 1.

There are also four Appendices, which contain details of various aspects of the model. Appendix A gives the model for the thermodynamic properties of equilibrium hydrogen used. This represents an improvement over the similar model described in Ref. 1, because it includes the lowering of the ionization potential, and a variable cut-off for the electronic partition function of the hydrogen atom.

Appendix B defines the absorption coefficient for 10.6 μm radiation in ionized hydrogen by inverse bremsstrahlung.

Appendix C gives the values for the thermal conductivity of equilibrium hydrogen used.

Appendix D describes briefly the radiation properties of hydrogen, and gives the expressions used for axial radiation transport of energy and for loss of energy by radiation.

2. ONE DIMENSIONAL LSC WAVE MODEL

2.1 Basic Equations

The LSC wave is described by an energy balance for the flowing gas and the incoming laser energy. The elements that make up this balance include absorption of laser energy, thermal conduction of energy, transport of energy by radiation, convection of energy, and loss of energy by radiation. The equation which expresses this balance is

$$\frac{d}{dx}(\rho u H) + \frac{dI}{dx} + \frac{d S_A}{dx} + P_T = \frac{d}{dx}\left(\lambda_C \frac{dT}{dx}\right) \tag{2.1}$$

Here ρ is gas density, u is gas velocity, H is gas total enthalpy ($h + u^2/2$) where h is the thermochemical enthalpy), I is the laser intensity, S_A the radiation energy flux, P_T the radiation loss term, and λ_C the equilibrium thermal conductivity of the gas. The terms in this energy equation are, respectively, convection, laser energy absorption, radiation energy transport, radiation energy loss and thermal conduction.

Conservation of mass is satisfied by the statement that the mass flow per unit area is a constant,

$$\rho u = \dot{m}_A = \text{constant} \tag{2.2}$$

Conservation of momentum is replaced by a constant pressure condition,

$$p = p_o \tag{2.3}$$

because the velocity changes are so small that pressure changes generated by momentum changes are negligible.

The laser absorption term is obtained from the laser energy transport term

$$dI/dx = - k_L I$$

where k_L is the absorption coefficient for the laser energy. The solution of this equation is

$$I = I_o e^{-\tau} \quad , \quad \tau = \int_0^x k_L \, dx \tag{2.4}$$

where τ is the optical depth and I_o is the incoming laser flux. Thus we find

$$dI/dx = - k_L I_o e^{-\tau} \tag{2.5}$$

The convection term, using (2.2), becomes

$$\frac{d}{dx} (\rho u H) = \dot{m}_A \left(\frac{dh}{dx} + u \frac{du}{dx} \right) \tag{2.6}$$

$$= \dot{m}_A \left(c_p \frac{dT}{dx} + \frac{\dot{m}_A^2}{\rho} \frac{d\rho^{-1}}{dx} \right)$$

The equation of state, (A-8), provides ρ in terms of T for the constant pressure p_o as

$$\rho^{-1} = R_M Z T / p_o \tag{2.7}$$

where R_M is the molecular gas constant, and Z is the compressibility factor. Differentiation gives

$$\frac{d}{dx}(\rho u H) = \dot{m}_A \left[c_p + \left(\frac{\dot{m}_A R_M}{p_o} \right)^2 Z^2 T \left(1 + \frac{d\ell nZ}{d\ell nT} \right) \right] \frac{dT}{dx} \qquad (2.8)$$

As discussed in Appendix D, we will use the conduction approximation for the radiation transport so that

$$\frac{d S_A}{dx} = - \frac{d}{dx} \left(\lambda_R \frac{dT}{dx} \right) \qquad (2.9)$$

where λ_R is radiation conductivity.

Use of (2.5), (2.8) and (2.9) enables us to express the energy equation as

$$\dot{m}_A \left[c_p + \left(\frac{\dot{m}_A R_M}{p_o} \right)^2 Z^2 T \left(1 + \frac{d\ell nZ}{d\ell nT} \right) \right] \frac{dT}{dx}$$

$$- k_L I_o \bar{e}^{\tau} + P_T = \frac{d}{dx} (\lambda_C + \lambda_R) \frac{dT}{dx} \qquad (2.10)$$

The quantities Z, $d\ell nZ/d\ell nT$, c_p, k_L, λ_C, λ_R and P_T are given in the Appendices as functions of T for a given $p = p_o$. They appear in Eqs. (A-19) (A-20), (B-4), (C-1) and Table C1, (D-9) and (D-1). Then (2.10) is a second order differential equation for T(x), the temperature distribution in the LSC wave. When suitable boundary conditions are imposed, it can be solved.

One set of boundary conditions can be obtained from the incoming flow at $x = -\infty$. However, one cannot solve the equations numerically starting at the incoming conditions, because these conditions are a solution to the equation and the numerical procedure will not move off that solution. Instead, one can integrate (2.1) from $x = -\infty$ where the initial conditions prevail, to $x = 0$, which is an arbitrary location, except that our definition of τ, (2.4), provides that no absorption of laser energy has yet occurred there. Denoting conditions at $x = 0$ by subscript i, we have

$$\dot{m}_A \left[h_i - h_o + (u_i^2 - u_o^2)/2\right]$$

$$+ \int_{-\infty}^{0} P_T dx = (\lambda_C + \lambda_R)_i \left(\frac{dT}{dx}\right)_i$$

The term on the right side at $x = -\infty$ has been set to zero since the temperature gradient is zero there.

We now assume that the temperature T_i is low enough at $x = 0$ so that no radiation losses have occurred yet, thus ignoring the integral over P_T. Replacing u by the mass conservation and state equations yields

$$\dot{m}_A \left[h_i - h_o + \left(\frac{\dot{m}_A R_M}{p_o}\right)^2 \frac{(Z_i^2 T_i^2 - T_o^2)}{2}\right] = (\lambda_C + \lambda_R)_i \left(\frac{dT}{dx}\right)_i \quad (2.11)$$

The enthalpy in (2.11) is given as a function of T in (A-27). For a chosen initial temperature T_i, (2.11) specifies $(dT/dx)_i$, and these give the two boundary conditions necessary to integrate the second order equation (2.10). The result should be independent of the choice of T_i, as long as it is low enough so that no significant laser energy absorption and no significant

radiation energy loss have yet occurred. This can be checked by performing the integrations for several values of T_i and verifying that the results do not change.

2.2 Scheme for Numberical Solution

The integration requires the specification of the mass flow constant $\dot{m}_A$ for a given laser flux I_o. As previous studies of LSC waves have shown, the integration of the energy equation is an eigenvalue problem. There is only one value of $\dot{m}_A$ for a given I_o which allows a physically realistic solution. This is related to the downstream conditions at the back of the LSC wave, as shown in Fig. 2.1. If $\dot{m}_A$ is too high, say $\dot{m}_{AU}$, the temperature profile will either rise indefinitely or peak, fall, and then rise again. This indicates that there is so much mass flow that the laser energy cannot heat it all, and an energy source is present downstream. On the other hand, if the mass flow is too low, say $\dot{m}_{AL}$, the temperature profile will rise to a peak, and then fall rapidly to zero, indicating the presence of an energy sink downstream. Only one value of $\dot{m}_A$ will permit the temperature to reach a finite value far downstream, and the integration must be performed so as to find this value.

We use an iterative scheme for this purpose. First, integrations are performed for several values of $\dot{m}_A$, until a pair of bounds are found, of which the upper bound causes the temperature to rise again after peaking and decreasing, and the lower bound causes the temperature to fall continuously after the peak. These two are then used in a bounding scheme. Their average is used for an integration. If it behaves as $\dot{m}_{AU}$, it is taken as the new upper bound, and if it behaves as $\dot{m}_{AL}$ it becomes the new lower bound. We continue to perform integrations, always using the average of the closest upper and lower bounds as the next value of $\dot{m}_A$. Eventually, $\dot{m}_{AU}$ and $\dot{m}_{AL}$ agree to as many significant figures as we like, and the corresponding

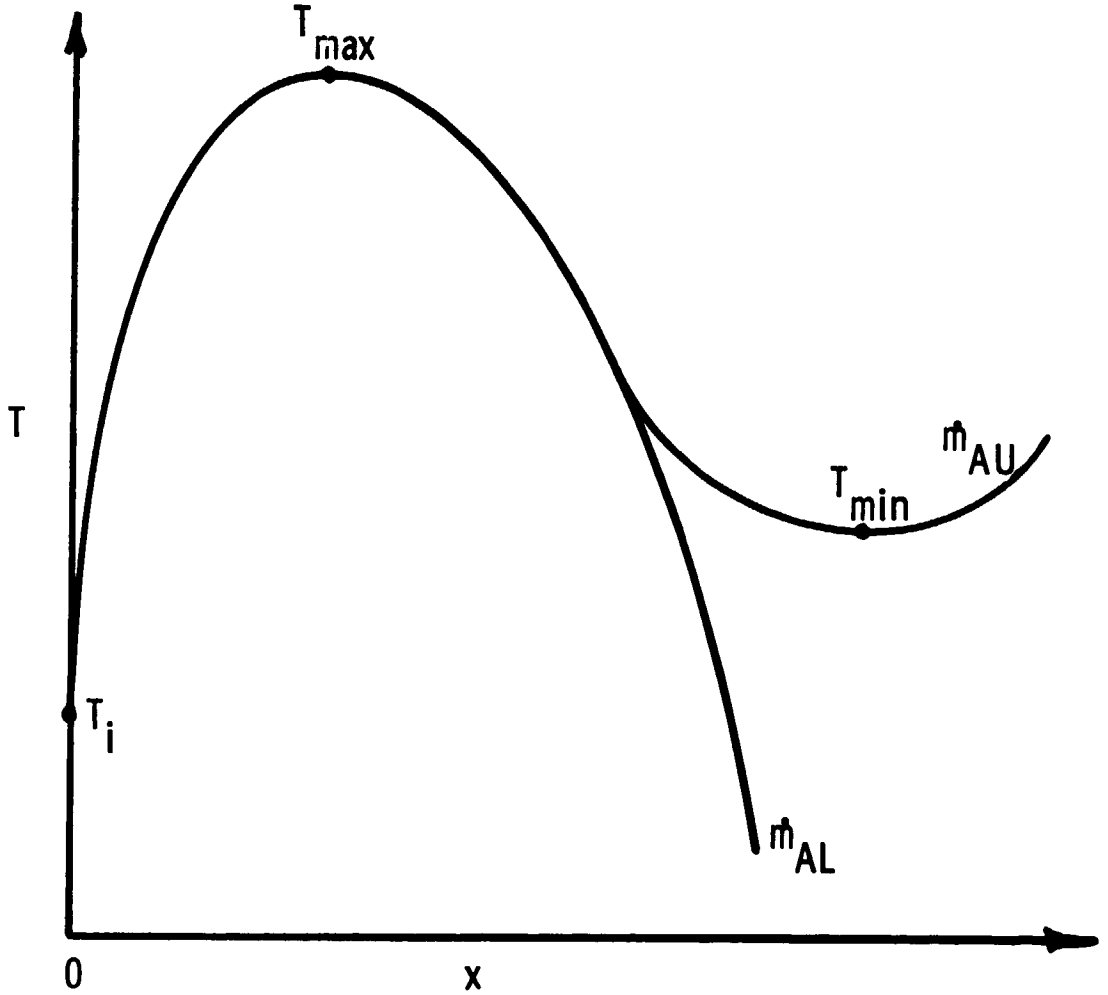

Fig. 2.1 Sketch of the Temperature Profile in an LSC Wave, Showing Upper and Lower Limit Curves.

temperature profiles agree very closely to some value of x, after which they diverage as shown in Fig. 2.1. The common value of $\dot{m}_{AU} \approx \dot{m}_{AL}$, and the common temperature profile is the solution sought.

Notice that we never are able to attain a profile which approaches a finite asymptotic temperature as $x \to \infty$. This would require infinite precision in $\dot{m}_A$. However, in our model there is no real significance to this asymptote. If we could find it, its value would depend on the low-temperature details of the radiation energy transport and loss, which are not accounted for correctly in our model anyway. Our procedure provides $\dot{m}_A$, the temperature profile in the region of high temperature, the absorption of laser energy, and the radiation losses, which are the important features of the LSC wave. The low temperature tail has no real significance.

The integration is performed using a standard 4th order Runge-Kutta integration scheme for a system of first order equations. The present system of equations is written in that way by defining a new variable W by

$$\frac{dT}{dx} = \frac{W}{\lambda_C + \lambda_R} \tag{2.12a}$$

Then (2.10) is

$$\frac{dW}{dx} = \frac{\dot{m}_A W}{\lambda_C + \lambda_R}\left[c_p + \left(\frac{\dot{m}_A R_M}{p_o}\right)^2 Z^2 T\left(1 + \frac{d\ell nZ}{d\ell nT}\right)\right]$$

$$- k_L I_o e^{-\tau} + P_T \tag{2.12b}$$

where, from (2.4)

$$\frac{d\tau}{dx} = k_L \qquad (2.12c)$$

This is a third order system for T, W, τ, whose boundary conditions are

$$x = 0: \; T = T_i, \; \tau = 0 \qquad (2.13a)$$

and from (2.14)

$$W_i = \dot{m}_A \left[h_i - h_o + \left(\frac{\dot{m}_A R_m}{p_o} \right)^2 \left(\frac{Z_i^2 T_i^2 - T_o^2}{2} \right) \right] \qquad (2.13b)$$

The parameters necessary to integrate this system are I_o, $\dot{m}_A$, T_i, p_o, T_o, and the radius R_i of the plasma tube. This latter parameter enters because the radiation loss P_T and the radiation conduction coefficient λ_R depend on R_i as described in Appendix D. R_i is found by choosing the laser power P and relating it to the intensity and area of the plasma tube as

$$P = I_o \pi R_i^2 , \quad R_i = (P/I_o \pi)^{1/2} \qquad (2.14)$$

2.3 Results

Calculations were performed for pressure levels of 1, 3, 10 and 30 atm, for powers of 10 kW and 5 MW. The temperature T_o of the incoming flow was taken as 300K. The incoming enthalpy for H_2, referenced to molecular hydrogen at 0K as the zero of enthalpy, is

$$h_o = 1.4466 \times 10^4 \, T_o \; (J/kg)$$

The gas constant for molecular hydrogen is $R_M = 4133$ J/kgK

The radiation loss term P_T requires specification of the constants C_3 and C_2, Eq. (D-1). They are functions of pressure p_o and plasma size R_i. However, they have only been worked out for certain sizes and pressures, as described in Appendix D. Calculations could be carried out for other values of R_i and p_o if required. Therefore, the values used in these calculations were the ones listed in the following table:

P (kW)	p_o (atm)	C_3	C_2
10	1, 3	2	2.4
10	10, 30	1.3	2.4
5000	1, 3	2	0.4
5000	10, 30	2.2	0.4

The initial temperature T_i was usually chosen as 10,000K, though some check runs were made at lower values, and for some low intensity cases lower values were used, because the peak temperature was near to or lower than 10,000K.

The integrations were performed with a step size in x which permitted the temperature to change by a maximum of 5% in one step, but there was also a specified upper limit on step size (DXMAX) to maintain accuracy. This varied with pressure, since the thickness of the wave was mainly determined by the absorption length, which decreases with increasing pressure.

An important property of the wave is the amount of laser energy absorbed. For low laser intensities, the gas is not heated to a high enough temperature to absorb all the energy, which defeats the purpose of the wave in the propulsion applications of interest here. A useful measure of energy absorption is the percentage of I_o absorbed by the

wave when the temperature has reached the minimum value T_{min} on the $\dot{m}_{AU}$ curve shown in Fig. 2.1. Very little additional absorption can occur after this point.

Table 2.1 gives the results of the calculations for the one-dimensional LSC wave model, in terms of the input parameters p_o, I_o, R_i, T_i, DXMAX, and the output parameters T_{max}, T_{min}, $\dot{m}_A$, u_e; and % I_o Absorbed. Here u_o is the incoming gas velocity, which is related to the mass flow per unit area and the incoming gas density ρ_o by (2.2) as

$$u_o = \dot{m}_A/\rho_o \qquad (2.15)$$

The first point to note in Table 2.1 is that the value of T_i does not affect the results as long as it is well below the peak temperature, and below the temperature at which laser absorption and radiation loss occur. This can be seen by comparing Cases 5' and 9, which show almost the same results for values of T_i = 10,000 K and 5000 K. A similar comparison is made for cases 31 and 32 for a 1000 K change in T_i. This result is to be expected, since the condition (2.11) applied at the initial station is an exact integral of the energy equation (2.10) if the absorption and loss terms are neglected. The only difference that could occur for two different choices of T_i is a displacement of the origin of x, which is located where $T = T_i$. However, if the origin is shifted to the same value of T for two cases with different values of T_i, the profiles cannot be distinguished.

An example of a temperature profile is shown in Fig. 2.2 from Case 3. The wave at this low pressure is more than 11 cm thick from the 10,000 K point. The divergence between the upper and lower limit mass flows begins at 10.6 cm. The upper limit profile begins to rise at 11.6 cm, 15,000 K, while the lower limit profile drops rapidly after 14,600 K at 11.6 cm, crossing T = 0 before 12 cm. The mass flows

TABLE 2.1

RESULTS OF ONE-DIMENSIONAL LSC WAVE MODEL

Case	I_o (W/cm^2)	R_i (cm)	T_i (10^3 K)	DXMAX (cm)	T_{max} (10^3K)	T_{min} (10^3K)	$\dot{m}_A$ (g/cm^2s)	u_o (cm/s)	% I_o Absorbed
P = 5 MW, p_o = 1 atm, ρ_o = 8.19E-5 g/cm^3, C_3=2, C_2 = 0.4									
1	1E6	1.26	10	.5	20.8	18.0	.367	4516	100
2	3E5	2.30	10	.5	19.1	16.4	.107	1303	100
3	1E5	3.99	10	.5	17.5	15.0	.0312	381	100
4	3E4	7.28	10	.5	15.5	12.8	.0648	79.0	93
5'	1.5E4	10.3	10	.1	14.0	11.7	.00191	23.3	75
9	1.5E4	10.3	5	.1	14.0	11.5	.00192	23.3	75
8	1E4	12.6	10	.5	12.9	10.8	.000727	8.87	59

Case	I_o (W/cm^2)	R_i (cm)	T_i (10^3K)	DXMAX (cm)	T_{max} (10^3K)	T_{min} (10^3K)	$\dot{m}_A$ (g/cm^2s)	u_o (cm/s)	$\%I_o$ Absorbed
P = 5 MW, p_o = 3 atm, ρ_o = 2.46E-4 g/cm^3, C_3=2, C_2=0.4									
12'	1E6	1.26	10	.05	20.8	18.6	.408	1660	100
13'	3E5	2.30	10	.1	19.0	17.0	.123	500	100
14'	1E5	3.99	10	.1	17.4	15.0	.0390	159	100
15"	3E4	7.28	10	.1	15.4	12.6	.00904	36.8	94
16"	1E4	12.6	10	.1	12.9	10.7	.00128	5.23	69
31	6E3	16.3	6	.1	11.4	10.1	.000458	1.86	56
32	6E3	16.3	7	.1	11.4	10.1	.000457	1.86	55
33	3E3	23.0	6	.1	9.9	9.5	.000146	.59	33
P=5MW, p_o = 10 atm, ρ_o = 8.19E-4 g/cm^3, C_3=2.2, C_2= 0.4									
26	1E6	1.26	10	.01	20.6	19.1	.482	588	100
27	3E5	2.30	10	.01	19.0	17.1	.157	192	100
28	1E5	3.99	10	.01	17.3	14.3	.0536	65.4	100
29	3E4	7.28	10	.01	15.2	12.0	.0134	16.4	96
30	1E4	12.6	10	.01	12.8	10.4	.00251	3.05	81

Case	I_o (W/cm^2)	R_i (cm)	T_i (10^3K)	DXMAX (cm)	T_{max} (10^3K)	T_{min} (10^3K)	$\dot{m}_A$ ($g/cm^2 s$)	u_o (cm/s)	$\%I_o$ Absorbed
P = 5 MW, p_o = 30 atm, ρ_o = 2.46E-3 g/cm^3, C_3 = 2.2, C_2 = 0.4									
38	1E6	1.26	10	.01	20.4	19.3	.609	248	100
24	3E5	2.30	10	.01	18.6	16.7	.210	85.4	100
23'	1E5	3.99	10	.01	16.9	14.1	.0745	30.3	100
22'	3E4	7.28	10	.01	14.7	10.9	.0200	8.14	99
21'	1E4	12.6	10	.01	12.5	10.0	.00471	1.92	92
P = 10 kW, p_o = 1 atm, ρ_o = 8.19E-5 g/cm^3, C_3 = 2, C_2 = 2.4									
111	1E6	.0564	10	.1	>30*	-	.121	1482	100?
112	3E5	.103	10	.1	23.4	16.6	.0447	546	96
113	1E5	.178	10	.1	16.3	13.4	.00952	116	79
114	3E4	.326	8	.1	11.3	10.9	.000412	5.04	20

*Temperature exceeded 30,000K, which is outside the range of conductivities available in the computer program.

Case	I_o (W/cm^2)	R_i (cm)	T_i (10^3K)	DXMAX (cm)	T_{max} (10^3K)	T_{min} (10^3K)	$\dot{m}_A$ ($g/cm^2 s$)	u_o (cm/s)	$\%I_o$ Absorbed
P = 10 kW, p_o = 3 atm, ρ_o = 2.46E-4 g/cm^3, C_3 = 2, C_2 = 2.4									
101	1E6	.0564	10	.05	26.6	18.5	.252	1027	100
103	3E5	.103	10	.05	19.0	15.2	.0730	297	99
105	1E5	.178	8	.05	15.6	12.6	.0164	66.8	84
107	3E4	.326	8	.05	11.7	10.6	.00105	4.26	40
109	2E4	.399	8	.1	10.6	10.2	.000470	1.91	25
108	1E4	.564	8	.05	9.3	9.2	.000149	.607	13
P = 10 kW, p_o = 10 atm, ρ_o = 8.19E-4 g/cm^3, C_3 = 1.3, C_2=2.4									
120	1E6	.0564	10	.01	20.9	18.1	.418	510	100
121	3E5	.103	10	.01	18.3	15.7	.129	158	100
122	1E5	.178	10	.01	16.2	13.2	.0349	42.6	95
123	3E4	.326	10	.01	13.1	10.9	.00468	5.72	71
124	1E4	.564	8	.01	10.4	9.9	.000796	.972	43

Case	I_o (W/cm^2)	R_i (cm)	T_i (10^3K)	DXMAX (cm)	T_{max} (10^3K)	T_{min} (10^3K)	$\dot{m}_A$ (g/cm^2s)	u_o (cm/s)	$\%I_o$ Absorbed
P = 10 kW, p_o = 30 atm, ρ_o = 2.46E-3 g/cm^3, C_3 = 1.3, C_2 = 2.4									
130	1E6	.0564	10	.01	20.4	18.0	.567	231	100
131	3E5	.103	10	.01	18.0	14.6	.178	72.5	100
132	1E5	.178	8	.01	15.7	11.1	.0526	21.4	98
133	3E4	.326	8	.01	12.9	10.3	.00994	4.05	86
134	1E4	.564	8	.01	10.7	9.6	.00218	.887	71

$\dot{m}_A$ for these upper and lower limit profiles differ by about 1.44E-4 percent! The temperature rise at the front of the wave is quite steep, rising from 10,000 K to 15,000 K in about 0.1 cm. This rise is caused by heating of the oncoming gas through the mechanisms of thermal and radiative energy transport. Only about 4% of the laser energy has been absorbed by the 15,000 K point. The major absorption occurs between there and the maximum temperature point, 17,500 K at 2.6 cm. By this point 73% of the laser energy has been absorbed. The high temperature region is quite broad, with more than 4.5 cm above 17,000 K. After that, there is a gradual fall as the radiation losses exceed the heating due to the combined effects of further absorption and energy transport by conduction and convection. The absorption is 99% complete at 8.6 cm, where the temperature has fallen to 16,000 K.

The very steep rise in temperature at the leading edge of the wave predicted by the present model should be viewed with some caution. The radiation conduction approximation is not really valid in regions of such steep temperature changes, so the details of the wave there may not be described correctly. However, energy is properly conserved in the model, so the details of the leading edge profile should not affect the subsequent features of the wave. In fact, observations of the temperature profile of LSC waves in air do show temperature gradients of the order of that shown in Fig. 2.2 (Refs. 8 and 9) so the present model is at least qualitatively in agreement with observation, even if the exact profile is in some doubt.

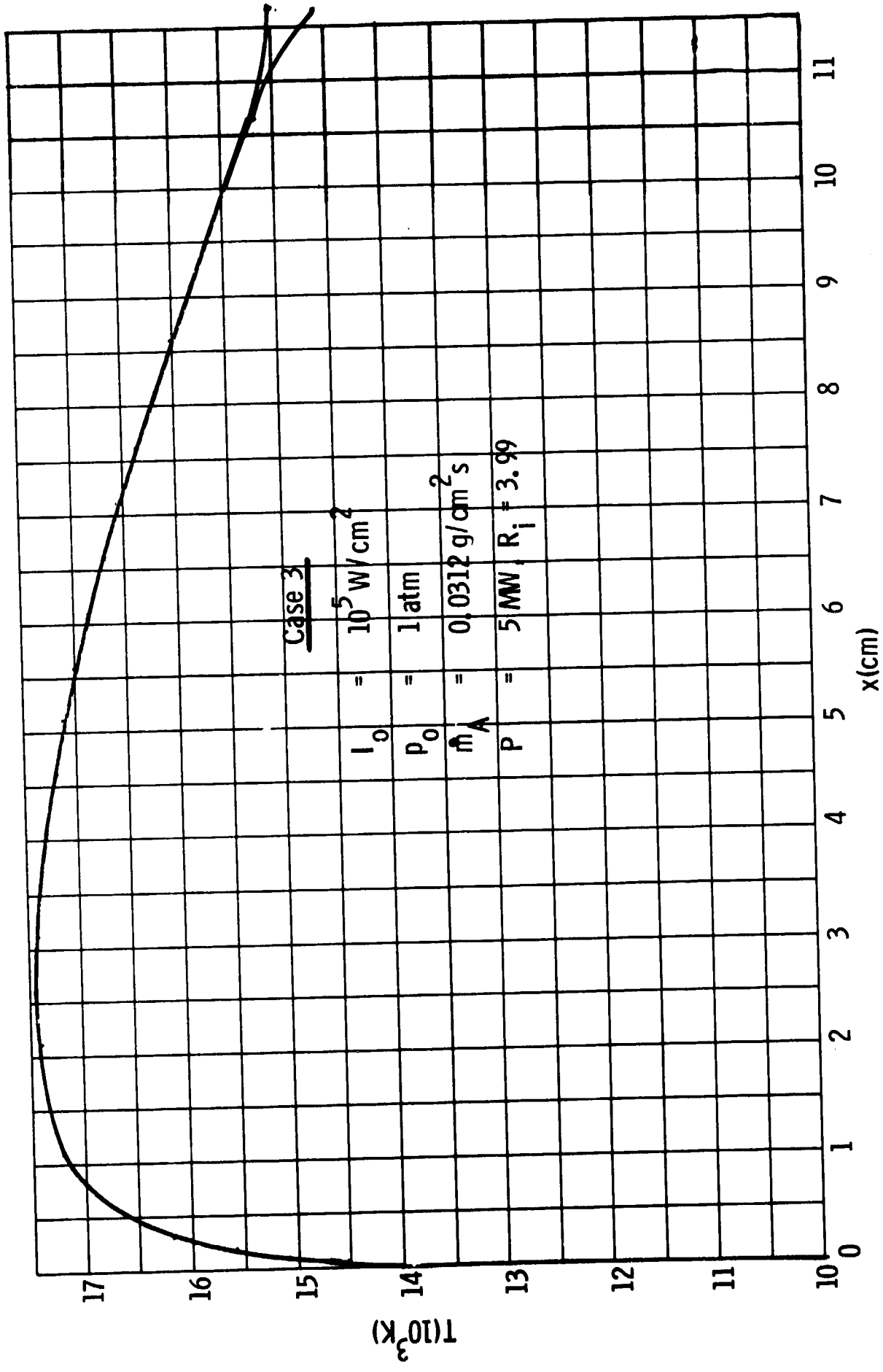

Fig. 2.2 Temperature Profile in LSC Wave

The general features of the temperature profile shown in Fig. 2.2 are typical of all the cases calculated. They all rise sharply, have a peak which is broad relative to their total thickness, and then fall gradually. The most notable differences are related to pressure and intensity. The higher the intensity, the higher the maximum temperature, almost independent of pressure. The pressure, on the other hand, strongly effects the thickness of the wave, because the absorption coefficient controls the rate of absorption of laser energy, and this coefficient is strongly pressure-dependent, see Appendix B. The higher the pressure, the thinner the wave, For example, Case 23' is the same as Case 3 but at 30 atm The peak temperature, 16,900 K, is reached 0.032 cm past the 10,000 K point, instead of 2.6 cm past, as with Case 3. The 15,000 K point is at 0.092 cm rather than 11.6 cm. The factor of 30 in pressure compresses the thickness scale of the wave by a factor of 100.

Perhaps the most important result of LSC wave calculations is the relation between intensity and mass flow. For a given value of I_o, the resulting value of $\dot{m}_A$ calculated provides the wave speed u_o at which the incoming gas must flow, according to (2.15). For the P = 5 MW case a plot of I_o vs $\dot{m}_A$ is shown in Fig. 2.3a, while a similar plot for the P = 10 kW case is shown in Fig. 2.3b. On these figures there is a line for each pressure, 1, 3, 10, 30 atm. The use of $\dot{m}_A$ rather than u_o permits the curves for all pressure levels to appear on the same graph. To give a feeling for the velocities u_o, the top horizontal scale is the velocity for 3 atm. Other velocities can be obtained easily, since they are inversely proportional to the pressure. The velocities are listed in Table 2.1. Also marked on the figure is the percent of laser energy absorbed in the wave, if it is less than 100%.

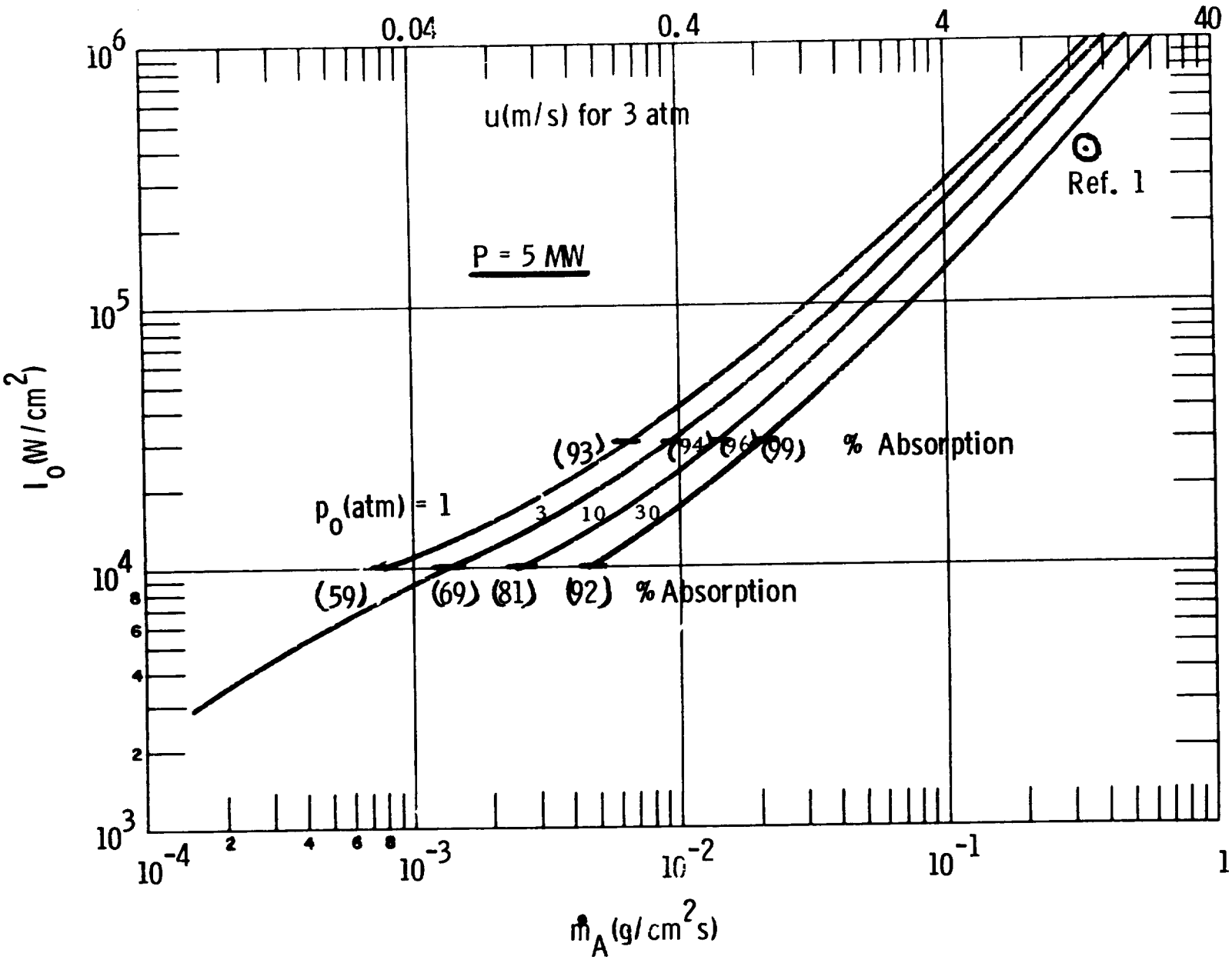

Fig. 2.3a Intensity vs Mass Flow for a Steady LSC Wave – P = 5 MW.

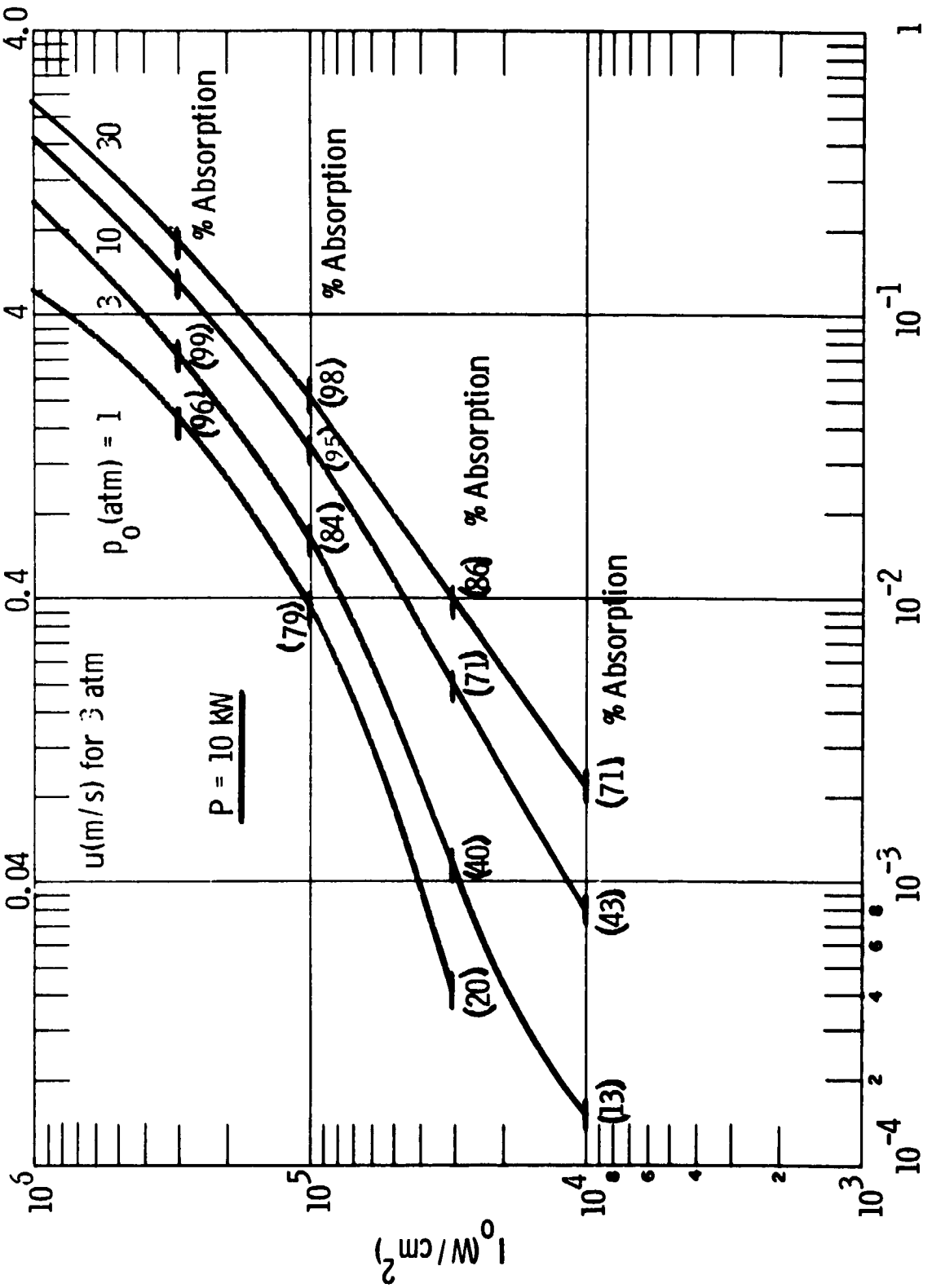

Fig. 2.3b Intensity vs Mass Flow for a Steady LSC Wave – P = 10 kW.

From Fig. 2.3we see that the pressure effect on $\dot{m}_A$ is not large at any I_o, varying from a factor of 2 for 5 MW at 10^6 W/cm^2 to a factor of 25 for 10 kW at 3E4 W/cm^2, when the pressure changes by a factor of 30.

At the higher intensities, $\dot{m}_A$ is approximately proportional to I_o, on the log-log scale, and this dependence persists, for 5 MW, down to 3E4 W/cm^2, which is the intensity region in which more than 90% of the laser energy is absorbed. Below 3E4 W/cm^2 the mass flow changes more rapidly than the first power of intensity. For 10 kW, the proportionality also holds where more than 90% of the laser energy is absorbed. The curves bend toward lower $\dot{m}_A$ at higher intensities for the 10 kW case than for the 5 MW case.

If attempts are made to calculate $\dot{m}_A$ for lower and lower intensities, eventually the values of $\dot{m}_A$ get very low and finally, no positive value will provide a solution which gives an upper limit type of curve for the temperature. This is indicative of the threshold phenomenon which has been found previously for LSC waves in air. There is some mass flow below which the wave cannot be sustained. No attempt was made to find this threshold in the present 1-D model for several reasons. First, losses may become important near the threshold, and the losses due to radial heat conduction are not included here, They are included approximately in the model described in section 4.1 and are there shown to have a large effect on the threshold in some cases. Second, the mass flows near threshold are very low, and it is felt that values below 10^{-4} g/cm^{2}s are not very interesting. Third, the fraction of laser energy absorbed near threshold may be very small. Since the main thrust of the present work is toward heating the gas, there is no real interest in dealing with cases where the laser energy mostly penetrates the wave rather than being absorbed. Fourth, at low intensities the T_{max} in the wave

are near 10,000K, and at these temperatures the radiation conduction model is not a good approximation to the radiation energy transport, so the present model is not a satisfactory representation of the physical situation.

The 1-D model of an LSC wave described here can predict the wave structure and properties. The most uncertain aspect of this 1-D model is the choice of constants C_3 and C_2 in the radiation loss expression. They should be functions of both pressure and radius R_i, but such an extensive program of calculation to obtain them was beyond the scope of the present work. It is expected that more accurate values of these constants will produce only small quantitative changes in the results presented here. More serious limitations to the present results are imposed by the 1-D nature of the model. The effect of several 2-D phenomena are discussed in Section 4. For sufficiently large size plasmas, this 1-D model is probably applicable.

Whether this model realistically describes LSC waves in hydrogen can only be determined by comparison with experimental measurements of such features as T_{max} and $\dot{m}_A$. There are no experimental results for LSC waves in hydrogen available at the present time.

3. COUPLED LSC WAVE-STREAMTUBE FLOW

3.1 Basic Equations

The flow of the gas in the streamtube brings in two new phenomena not included in the 1-D LSC wave model. These are area changes and pressure changes. The purpose of the area change is to accelerate the gas, in order recover maximum momentum for purposes of propulsion.

With these new phenomena, all the equations of motion change. The mass conservation equation now includes the cross-sectional area A:

$$\rho u A = \dot{m} = \text{constant}, \quad A = \pi R^2 \tag{3.1}$$

The momentum conservation equation expresses the balance of pressure and inertia forces:

$$\frac{dp}{dx} + \rho u \frac{du}{dx} = 0 \tag{3.2}$$

The energy conservation equation must now include the area terms, so (2.1) is modified to

$$\frac{d}{dx}(\dot{m}H) + \frac{d}{dx}(AI) + AP_T = \frac{d}{dx}\left[A(\lambda_C + \lambda_R)\frac{dT}{dx}\right] \tag{3.3}$$

Here we have again used the conduction approximation for the radiation energy transport term.

The inclusion of the terms on the right in a streamtube calculation deserves some comment. Ordinarily, streamtube calculations do not include these axial conduction energy transport terms, and in fact they were

not included in the energy equation of Ref. 1. However, for LSC waves the temperatures are sufficiently high so that the radiation conduction coefficient λ_R is large, making the axial radiation transport significant even though the temperature gradients are not large. Once the radiation transport is included, the thermal conduction term can also be carried along with very little additional effort, and it also may be significant at the higher temperatures. The inclusion of these transport terms makes the energy equation second order in T, rather than first order, as it was in Ref. 1, so an additional boundary condition is needed.

The reduction of (3.3) to an equation in T and p is straightforward. Since the gas enthalpy is a function of these two variables, its derivative is

$$dh = c_p\, dT + c_T\, dp$$

$$c_p = (\partial h/\partial T)_p \quad , \quad c_T = (\partial h/\partial p)_T$$

With $\dot{m}$ constant, the first term of (3.3) can be written

$$\frac{d}{dx}(\dot{m}H) = \dot{m}\left(\frac{dh}{dx} + u\frac{du}{dx}\right)$$

$$= \dot{m}\left(c_p\frac{dT}{dx} + c_T\frac{dp}{dx} + u\frac{du}{dx}\right) \qquad (3.4)$$

The laser absorption term again follows from the energy transport equation

$$dAI/dx = k_L AI$$

$$AI = A_i I_o e^{-\tau} \quad , \quad \tau = \int_0^x k_L\, dx \qquad (3.5)$$

where A_i is the cross-sectional area of the LSC wave plasma. Then

$$d\,AI/dx = k_L A_i I_o e^{-\tau}$$

We also note that this nozzle flow starts at the back of the LSC wave so that $\dot{m} = \dot{m}_A A_i$. Then we can use (3.4) and (3.6) in (3.3) and divide by the constant $\dot{m}$ to get

$$c_p \frac{dT}{dx} + c_T \frac{dp}{dx} + u \frac{du}{dx} = \frac{-P_T}{\rho u} + \frac{d}{dx}\left[\left(\frac{\lambda_C + \lambda_R}{\rho u}\right)\frac{dT}{dx}\right] + \frac{k_L I_o e^{-\tau}}{\dot{m}_A} \quad (3.6)$$

Since ρ can be eliminated by the equation of state (2.7), we have three equations (3.1), (3.2) and (3.6) for the four variables p, T, u and A. When one of them is specified as a function of x, the other three can be determined. The conventional way to solve this problem is to specify a streamtube shape A(x) and solve for p, T, and u. However, as pointed out in Ref. 1, this method leads to a singular point when u equals the local sound speed, which makes the integration a difficult numerical problem. A much simpler integration can be done if u(x) is specified and the equations are solved for p, T and A (or $R = (A/\pi)^{1/2}$). This was the method used in Ref. 1 and it will also be used here.

To this end, (3.2) is used to write the left side of (3.6) as

$$c_p \frac{dT}{dx} + c_T \frac{dp}{dx} + u \frac{du}{dx} = c_p \frac{dT}{dx} + (1 - \rho c_T)\, u \frac{du}{dx}$$

The coefficient of the second term is given in Eq. (A-1) of Appendix A as

$$1 - \rho c_T = -(\partial \ln \rho / \partial \ln T)_p$$

and differentiation of the equation of state (2.7) gives

$$1 - \rho c_T = 1 + (\partial \ln Z / \partial \ln T)_p$$

Then the energy equation (3.6) is

$$c_p \frac{dT}{dx} + \left[1 + \left(\frac{\partial \ln Z}{\partial \ln T} \right)_p \right] u \frac{du}{dx} = \frac{-P_T}{\rho u} + \frac{k_L I_o e^{-\tau}}{\dot{m}_A}$$

$$+ \frac{d}{dx} \left[\left(\frac{\lambda_C + \lambda_R}{\rho u} \right) \right] \frac{dT}{dx} \qquad (3.7)$$

Equations (3.1), (3.2) and (3.7) are now three rather simple equations for p, T and R when u(x) is given. To them must be appended the definition of τ, (3.5). For computation they are written as a first order system by defining

$$V = \frac{\lambda_C + \lambda_R}{\rho u} \frac{dT}{dx} \qquad (3.8)$$

so the system becomes

$$\frac{dT}{dx} = \frac{\rho u V}{\lambda_C + \lambda_R} \qquad (3.9a)$$

$$\frac{dV}{dx} = \frac{c_p \rho u V}{\lambda_C + \lambda_R} + \left[1 + \left(\frac{\partial \ln Z}{\partial \ln T} \right)_p \right] u \frac{du}{dx} + \frac{P_T}{\rho u} - \frac{k_L I_o e^{-\tau}}{\dot{m}_A} \qquad (3.9b)$$

$$dp/dx = - \rho u \, du/dx \qquad (3.9c)$$

$$d\tau/dx = k_L \qquad (3.9d)$$

$$R/R_i = (\dot{m}_A/\rho u)^{1/2} \qquad (3.9e)$$

The density ρ is given by the state equation (2.7) and the thermodynamic derivative in (3.9b) is given in Appendix A, Eqs. (A-19a) and (A-19b).

The initial conditions on most of the variables are straightforward. One begins the integration at some value of x, where the values of T, u, p, τ are known from the LSC wave solution. If we denote the point where the streamtube solution is joined to the LSC wave solution by the subscript c, then we have

$$x = x_c: \quad T = T_c, \quad p = p_o, \quad \tau = \tau_c, \quad u = u_c$$

One further initial condition, on dT/dx, is needed. The specification of that condition is not so straightforward, and it is discussed next in connection with the description of the numerical method of solution.

Notice that we perform the integration in the physical distance variable x. In Ref. 1 we used the optical depth variable τ instead. This variable has some utility when the radiation transport terms are not included, because then k_L does not appear in the energy and momentum equations. It only serves to define the physical distance scale through (3.9d). However, in the present case, where P_T and the transport terms are included, there is no such simplification gained by using τ, and we chose to use x as the independent variable.

3.2 Numerical Method

The joining of the streamtube equations (3.9) to an LSC wave solution requires one more boundary, on dT/dx, in addition to those given in (3.10). If one merely picked a station x_c and used the value of dT/dx there, the streamtube solution would either rise or fall, just as the LSC wave solution did. One needs a degree of freedom for the streamtube integration corresponding to $\dot{m}_A$ in the LSC wave integration. This freedom is provided by dT/dx. Near the rear of the LSC wave solution the values of dT/dx (or

W, see Eq. (2.12a) ; are different for the upper and lower limit solutions, even though they correspond to solutions with nearly the same value of $\dot{m}_A$. Thus, dT/dx is only determined within some range. For example, in the case to be discussed here, Case 13', at x = 2.97 cm, the values of W differ by 17%. Thus, if we start a streamtube solution there, one may use any value of W between the two limits to obtain the initial value of dT/dx (or V, see Eq. (3.8)), and still be consistent with the LSC wave solution. With this degree of freedom available to us, we may set up a scheme for joining the streamtube calculation to an existing LSC wave solution.

First, we wish to choose a matching point x_c. It seems desirable to choose this as far toward the back of the LSC wave as possible, so that most of the gas heating and laser absorption occurs in the constant area wave, which acts as a "combustion chamber". We therefore choose the upper limit LSC wave solution, and choose a number of points near the end of the wave, before the minimum temperature point. At each point we integrate the streamtube equations, using the value of $V = W/\rho u = W/\dot{m}_A$ appropriate to that point. For smaller values of x, the resulting temperature profile will eventually rise. We find the smallest value of x for which it rises, and choose this as our matching point x_c.

We then integrate the streamtube equations again from this x_c, but this time we allow the initial value of W to vary, and we iterate on it to find upper and lower profiles of T, just as we did for $\dot{m}_A$ in the LSC wave solution. This integration will progress a certain distance in x, until the T profiles diverge, one to fall and one to rise. We then pick a point where T differs by only a few degrees on the upper and lower limit curves, start integrating there, and again iterate on V to find another pair of limit curves. We continue in this fashion, moving toward large x step-by-step for as long as we choose, to calculate the conditions in a streamtube matched to any given LSC wave solution.

The results of one sample calculation using this method are given below, and they show this to be a feasible scheme of calculation, which produces a consistent solution. There may, of course, be other schemes which also work. No attempt was made to find the most efficient scheme.

Before the results are given, we will describe the velocity distribution function chosen for our sample case. This function is a required input to the streamtube integration.

3.3 Velocity Distribution

The form of the function u(x) chosen will determine the shape of the streamtube R(x). Several conditions on u(x) are clearly desirable. At x_c, it should join smoothly on to the velocity in the LSC wave, where value u_c and slope $(du/dx)_c$ are known. It should increase to a high value since we wish to accelerate the flow in the streamtube, and in fact should reach the local speed of sound at about the location where the throat is desired.

There are clearly many functions u(x) which have these properties. Whether any given function is satisfactory can only be determined after the calculation is performed and the resulting streamtube shape determined to be a reasonable one.

For the sample calculation performed here, the velocity distribution was taken in the form

$$\frac{u}{u_c} = \exp\left[\frac{x - x_c}{u_c}\left(\frac{du}{dx}\right)_c\right] + a\left(\frac{x - x_c}{x_f - x_c}\right)^E \qquad (3.11)$$

The first term assures that u and du/dx have the values u_c and $(du/dx)_c$ at $x = x_c$, providing the power E on the second term is greater than unity. The second term provides the increase in u as x increases. Since the slope of u in the LSC wave is small at the joining point x_c, the value of u reached at $x = x_f$ will be nearly au_c. Thus the parameters a and x_f determine the velocity reached at some chosen station x_f.

The slope of this expression is

$$\frac{du}{dx} = \left(\frac{du}{dx}\right)_c \exp\left[\frac{x - x_c}{u_c}\left(\frac{du}{dx}\right)_c\right] + \frac{aE}{x_f - x_c}\left(\frac{x - x_c}{x_f - x_c}\right)^{E-1} \quad (3.12)$$

For the particular case calculated here, the joining point x_c was about 3 cm. The point x_f was chosen as 5 cm, and a was taken as 10 so that at x = 5 cm, the velocity would be approximately 10 times u_c. The exponent E was taken as 2. Changes in a, E, and x_f clearly will alter the length of the streamtube to the throat, as will its size and shape. Experience with the calculations should permit choosing the parameters so as to obtain any desired streamtube shape of reasonable form.

3.4 Results

The case used to illustrate the coupling calculation was Case 13', p_o = 3 atm, I_o = 3E5 W/cm^2, P = 5 MW. This was chosen as close to one of the cases calculated in Ref. 1.

The calculation was completed in 5 steps using the velocity distribution function described above. The course of the calculation is given in the following Table. The value of x at the beginning of each step is given, starting with x_c, the matching point to the LSC wave. The values of T_U, T_L, W_U and W_L on the upper and lower curves of the previous step are also given, as well as the value of W found by iteration for the step starting at x.

x(cm)	T_U(K)	T_L(K)	$W_U \times 10^{-6}$	$W_L \times 10^{-6}$	$W \times 10^{-6}$
2.9683	17,129	17,098	-47.37521	-56.84703	-50.48019
4.2183	16,509	16,508	-2.251405	-2.457159	-2.294881
4.6983	16,333	16,328	-1.638167	-3.242737	-1.814397
5.0183	16,168	16,167	-1.864034	-2.245204	-1.984559
5.2883	15,982	15,980	-1.817534	-2.539966	-2.341516

It is seen that the step sizes decrease as we approach the streamtube throat. The last step passed through the throat before the temperature began to rise, and the calculation was terminated with this step. The throat conditions were

$x = 5.5583$ cm, $T = 15,740$ K, $h = 1.308E9$ J/kg, $p = 1.77$ atm

$u = 15.07$ km/s, $R/R_i = 0.2943$, $R = 0.677$ cm, $M = 1.08$

The laser energy was completely absorbed, and in fact, at $x_c = 2.9683$ cm only 4.9E-3 percent of the laser was not absorbed, so the streamtube calculation could have proceeded with the laser absorption term.

Notice that the value of W resulting from the iteration at each step was between the upper and lower values for that location in the previous step, which testifies to the consistency of the calculation scheme. The uncertainty in W can be used to make the calculation progress downstream in a consistent manner.

Note that the Mach number M at the physical throat need not be unity when heat addition is occurring. The pressure is down from 3 to 1.77 atm, which is a little higher than the perfect gas ($\gamma = 1.4$) value of 1.58 atm, because of real gas effects. In connection with the pressure it should be noted that λ_C was only tabulated at specific pressures, and the present calculations were performed by using the value at the nearest pressure, rather than by interpolating. It would probably be somewhat more accurate to interpolate in pressure, at the expense of some complication in the program.

Plots of $T(x)$, $u(x)$ and $R(x)/R_i$ are given in Fig. 3.1. The temperature profile shows the characteristic rapid rise, peak and slow decay. The maximum is at 19,000 K at 0.5 cm. The tic marks on this curve, and the others, indicate the starting points for the integrations, as listed in the above table. In the streamtube portion of the flow, the temperature only drops from 17,129 K to 15, 740 K.

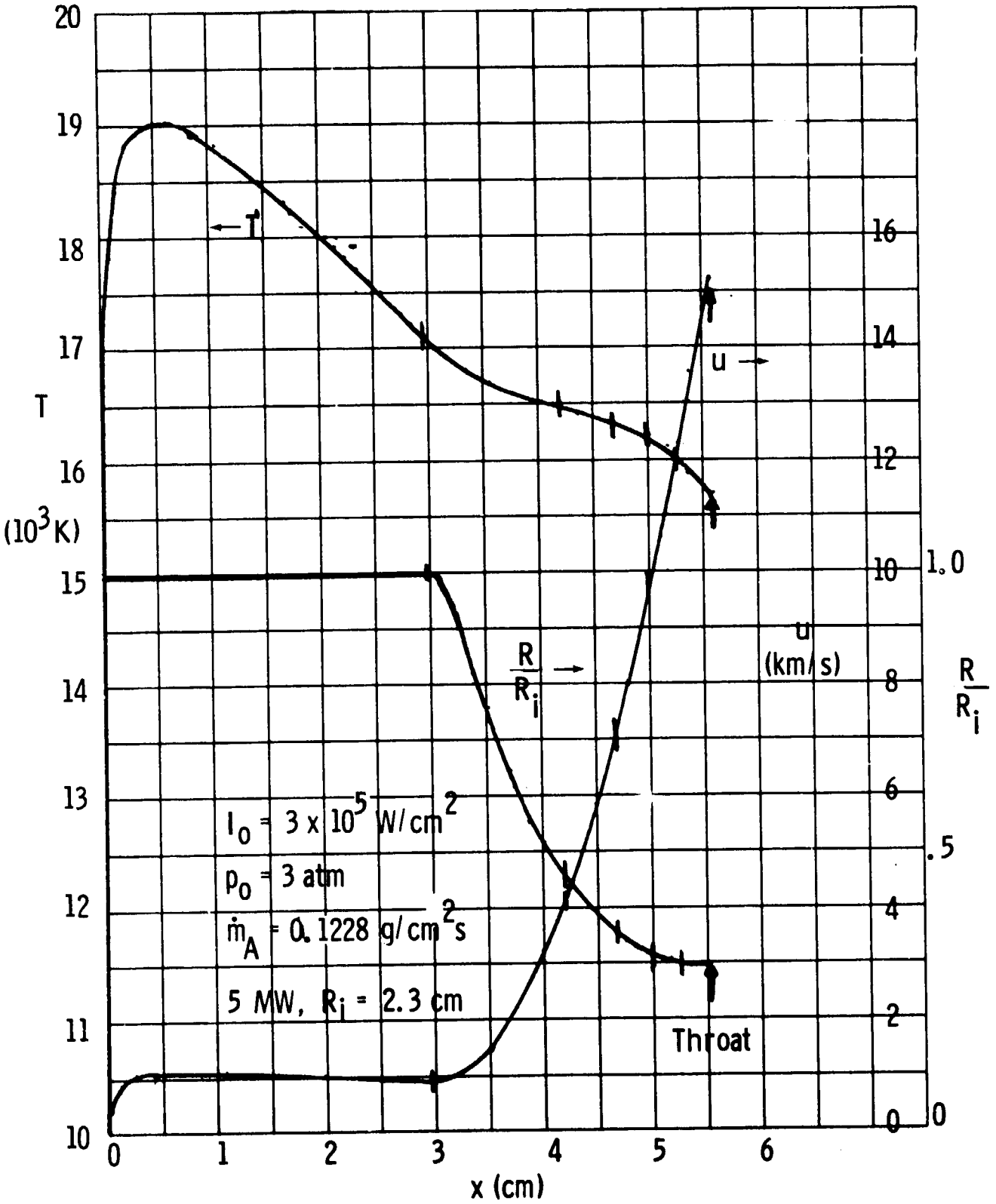

Fig. 3.1 Velocity, Temperature and Radius Distributions for Coupled LSC Wave-Streamtube Flow.

The velocity profile shows a rapid rise to the station of maximum temperature, and is then nearly flat, with a slow decrease, during the LSC wave. This corresponds to the density showing a slow increase, since ρu is constant. This is consistent with the temperature drop of 1400 K in this region, since p is constant, and the gas is fully ionized, so ρT is nearly constant. During the streamtube portion of the flow the velocity increases rapidly according to the relation given in (3.11) and the constants specified below (3.12). It reaches $10\ u_c$ at x_f = 5 cm, as specified and continues to increase to the throat.

The radius ratio remains at unity through the LSC wave, and then decreases in the streamtube region, reaching the throat value of 0.2943 at x = 5.56 cm. This shape could have been altered by changing the velocity distribution parameters. If x_f had been made larger, the streamtube would have been longer, probably with nearly the same throat size, but with a lower temperature due to the additional radiation losses brought about by the increased length.

For this calculation one can easily estimate the total radiation losses by finding the energy contained in the flowing gas at the throat. With the values of h and u given above, the total gas enthalpy is 1 308E9 + 0.5 $(1.507E4)^2$ = 1.42E9 J/kg. The mass flow per unit area in the wave is 1.228 kg/m^2s and the radius of the plasma in the wave is 0.023 m, so the total mass flow is $1.228\ \pi(0.023)^2$ = 2.04 E-3 kg/s. The total power flow through the throat is thus 2.90 MW, which is 58% of the input power. Thus 42% of the power has been lost in radiation.

This calculation may be compared with one of the cases in Ref. 1. There, the presence of the LSC wave was not considered, except to estimate the mass flow to support the wave by a very crude calculation of the wave structure. The result, for P = 5 MW, p_o = 3 atm, I_o = 3.67E5 W/cm^2, was $\dot{m}_A$ = 0.3316 g/cm^2s, a value plotted as the circle on Fig. 2.3a marked Ref. 1. It is a factor of 2.7 higher than the value of 0.1228 g/cm^2s calculated in the

present work for I_o = 3E5 W/cm^2. With this high value used, the calculation of the streamtube in Ref. 1 was carried out by using the equations of this section, but without the energy transport terms on the right of (3.3). The calculation was started at 12,000 K, with the laser energy reduced by the amount of energy necessary to heat the assumed mass flow to this temperature. The resulting temperature distribution is shown in Fig. 3.2, taken from Fig. 7.2a of Ref. 1. Without the presence of the LSC wave, and with nearly 3 times the mass flow, this profile shows a much different character than that of the present work, Fig. 3.1. It rises gradually to a peak of only 14,900K, and drops to 14,300K at the throat. The lower temperature is largely a result of the higher mass flow at nearly the same laser intensity. But lower temperature reduces the radiative losses, as does the shorter length of the flow, 3.2 cm instead of 5.5. The result is that the calculation in Ref. 1 of the radiation losses showed them to be only about 5% of the input power, rather than the 42% in the present more accurate calculation.

This comparison emphasizes the necessity of having a correct calculation of the mass flux through the LSC wave in order to properly obtain the temperature levels in the flow, and the resulting losses. Based on this example, the radiation loss calculations in Ref. 1 must be considered as doubtful. In order to assess them more accurately, streamtube calculations by the present method should be coupled to the LSC wave calculations described in Section 2. The single sample calculation described here shows that the present method can be used for this coupling.

The large losses found in the present calculation are attributable to the high temperature level in the gas. This in turn is caused by the necessity of having a significant degree of ionization, so that the absorption mechanism of inverse bremsstrahlung can operate. Ionization in hydrogen requires temperatures in excess of 10,000K. It would be advantageous to operate

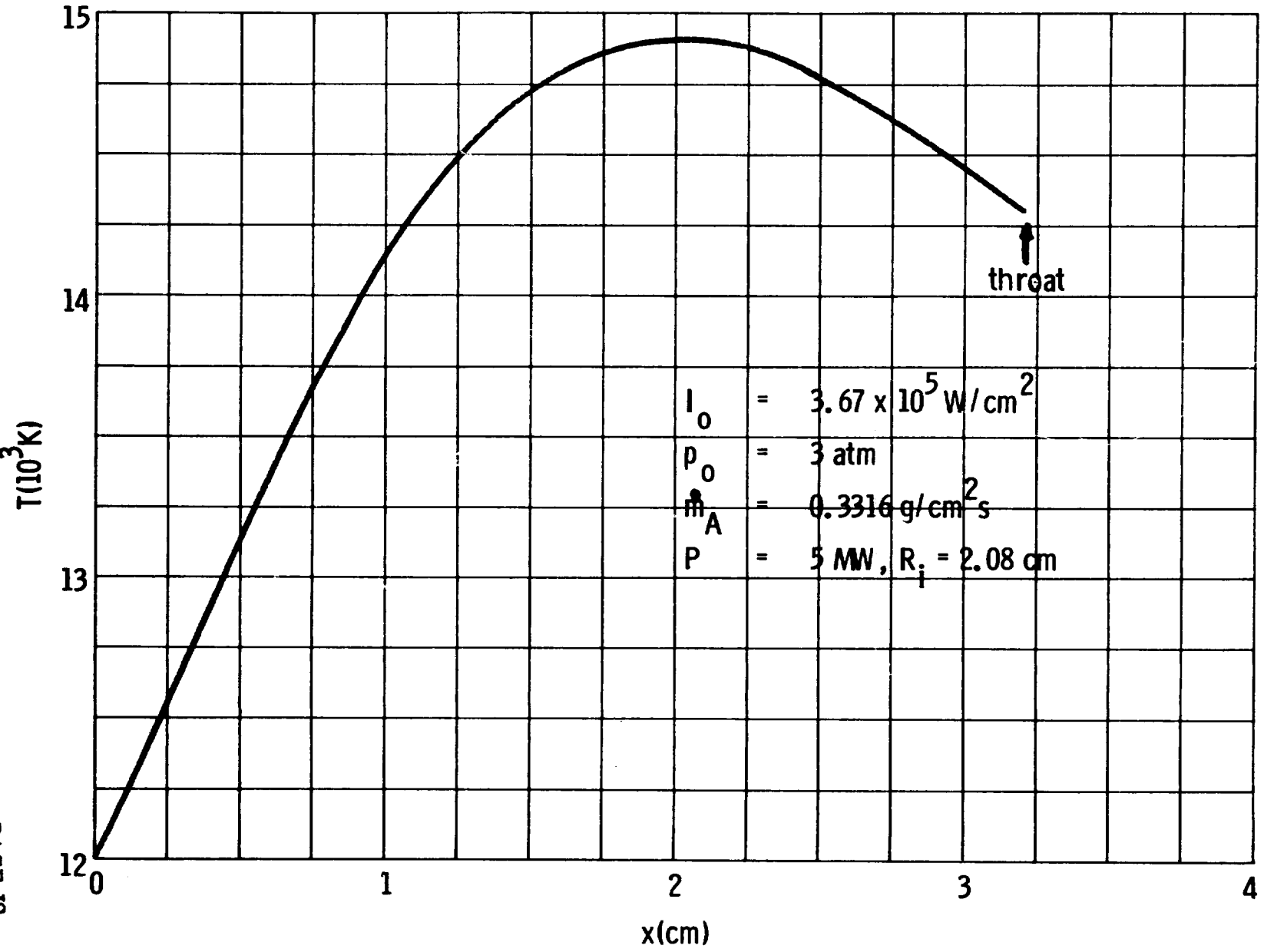

Fig. 3.2 Temperature Profile Obtained by Method of Ref. 1 (from Fig. 7.2a of Ref. 1).

at lower temperatures to reduce the losses. This could be achieved by using an easily ionizable seed in the hydrogen, to produce electrons at lower temperature. However, the type and amount of seed must be chosen with care. The weight of the seed will reduce the specific impulse of the gas, and so will the reduced temperature. It would be desirable to conduct a study similar to the present one, but using seeded hydrogen, to determine the effect on mass flux, specific impulse, and losses, of various types and amounts of seed.

4. TWO DIMENSIONAL EFFECTS

4.1 Heat Losses

One of the two-dimensional effects not included fully in the one-dimensional model is transverse (radial) heat loss from the plasma cylinder. The only loss of this type included is the radiation loss from small cylinders, where the plasma is transparent. For larger cylinders, the radial radiation loss also includes black radiation from the edges of the cylinder due to the radial temperature gradient, which is not accounted for in the one-dimensional model, as explained in Appendix D. And for all cylinder sizes, the transverse conductive loss has not been included. In this subsection we describe an estimate of these losses and show their effect on the $\dot{m}_A$ vs I_o relation.

To account for radial conduction losses a term

$$\frac{1}{r} \frac{\partial}{\partial r} \left(r \lambda_C \frac{\partial T}{\partial r} \right) = q_{rc} \tag{4.1}$$

has to be added to the right side of Eq. (2.1), where r is the cylindrical radial coordinate. To include this in the framework of the one-dimensional model one needs to express it as a function of x only. Let us assume q_{rc} depends on x only. We may then integrate (4.1) twice on r between the center of the cylinder r = 0 and the edge, R_i, to get

$$q_{rc} = \frac{-4}{R_i^2} \int_{T_e}^{T} \lambda_C \, d T \tag{4.2}$$

where T_e is the temperature at the edge of the cylinder.

An expression of the form (4.2) provides an estimate of the heat loss term which is to be added to the right side of (2.1) to account for transverse conduction loss. The value to use for T_e is not certain since we do not know the radial temperature profile. Since most of the integral is at high temperature, the value of the low edge temperature will not have much effect on q_{rc}, so we take $T_e = 300$ K, which gives the integral its largest value. To compensate for this we could reduce the factor 4 somewhat. In fact, (4.2) has already been suggested by Raizer in Ref. 2 to estimate the conduction losses, though he used 2.9 instead of 4. We adopted the value 3 in our calculations.

In addition to the conductive loss, there is also the radiation loss for large plasma cylinders, as mentioned above. If we use the radiation conduction approximation for this term, it is also of the form of (4.2), with λ_R instead of λ_C.

To use these estimates for assessing the effect of radiation losses we simply add to the right side of (2.12b) the terms

$$\frac{C_{LC}}{R_i^2} \int_{300}^{T} \lambda_C \, dT + \frac{C_{LR}}{R_i^2} \int_{300}^{T} \lambda_R \, dT \qquad (4.3)$$

The first integral is tabulated in Table C2, Appendix C as I_{λ_C}. It is a function of T and quadratic interpolation was used between the tabulated values of T. The second integral is tabulated in Table D1 of Appendix D as I_{λ_R} and was used in the same way.

Calculations were made including these loss terms by the same scheme described in Section 2.2, using the values

$$C_{LC} = 3, \quad C_{LR} = 3 \quad \text{for} \quad P = 5 \text{ MW}$$

$$C_{LC} = 3, \quad C_{LR} = 0 \quad \text{for} \quad P = 10 \text{ kW}$$

The results are shown in Fig. 4.1, which is a plot of I_o vs $\dot{m}_A$. The lines are the results for no sideways losses from Fig. 2.3, while the symbols show the results including losses. For the 5 MW power, Fig. 4.1a, there is very little effect of these losses, even at the highest intensities, where R_i is the smallest and the temperature the highest, which make the loss terms the largest. But for the 10 kW power, Fig. 4.1b, these losses show a large effect because of the small sizes involved. For 3 atm, solutions could be obtained only at I_o = 1E6 and 3E5 W/cm^2, but there was no solution which has $\dot{m}_A$ > 1E-4 g/cm^{2}s at I_o = 2E5. That intensity is marked as the 3 atm threshold on Fig. 4.1b. Similar thresholds are marked for 10 and 30 atm. For p_o = 1 atm, no such solution was found even at 1E6 W/cm^2. Thus, when the losses are included, thresholds are found much above the intensities at which they would have been found without losses, for the 10 kW power.

Where solutions were found, they occur at lower mass flow for a given intensity. The reductions in mass flow are quite small at the higher pressure, but are large at the lower pressure; at 3 atm the reduction is about a factor of 2. This large effect at low pressure is caused by the large length of the wave, which allows more area to contribute to the radial heat loss.

This limited set of calculations, which is tabulated in Table 4.1, shows the importance of including the transverse loss when considering small sizes and low pressures. The effects found are believed to be qualitatively accurate, but probably not quantitatively precise. The expressions (4.3) are of the correct form, and have the correct dependence on radius, but they are one-dimensional approximations to a two-dimensional phenomenon, and contain coefficients C_L which can only be estimated roughly. A more precise evaluation of the transverse heat loss due to thermal condition and black radiation requires a two-dimensional model of the wave.

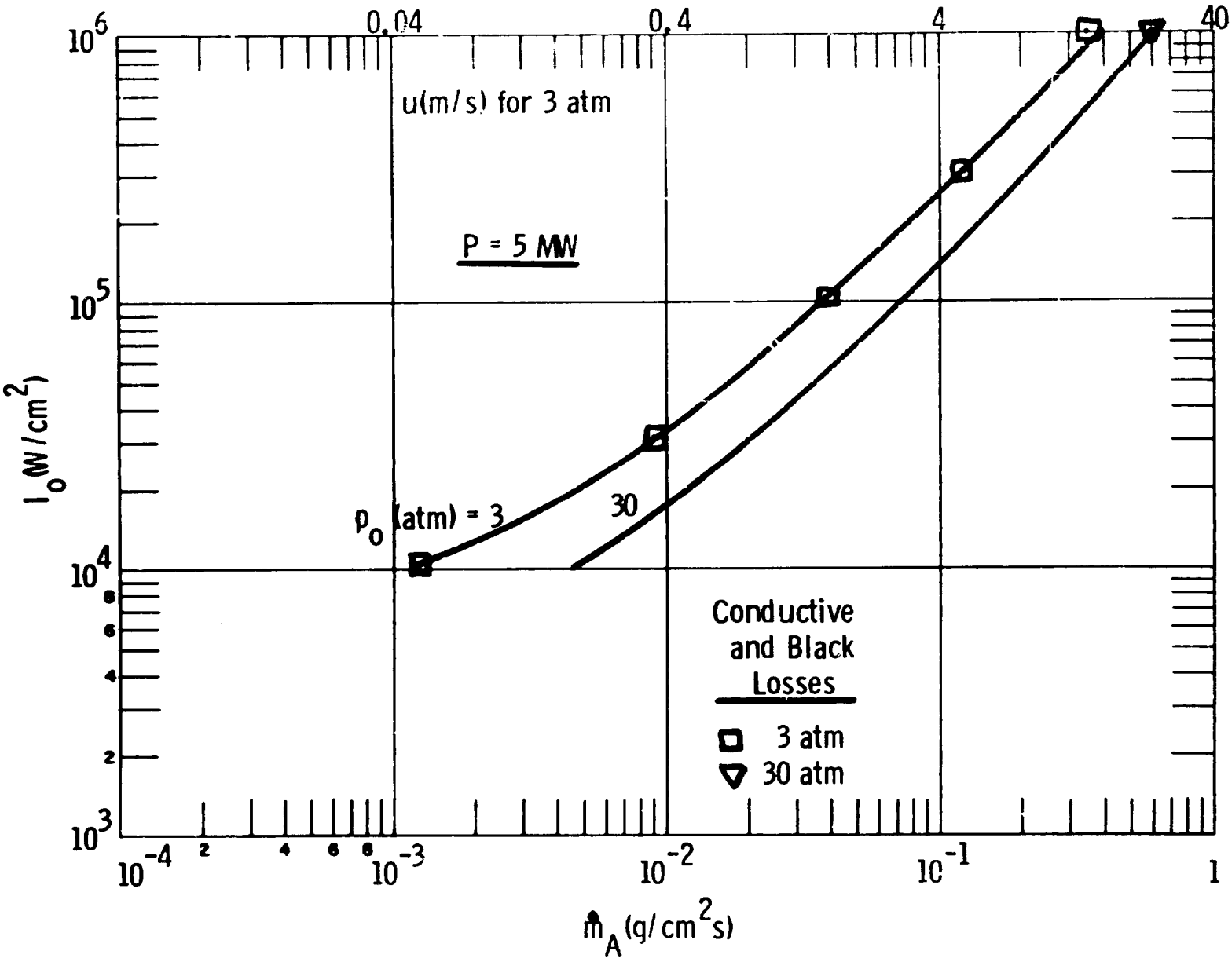

Fig. 4.1a Intensity vs Mass Flow for a Steady LSC Wave with Radial Loss – P = 5 MW.

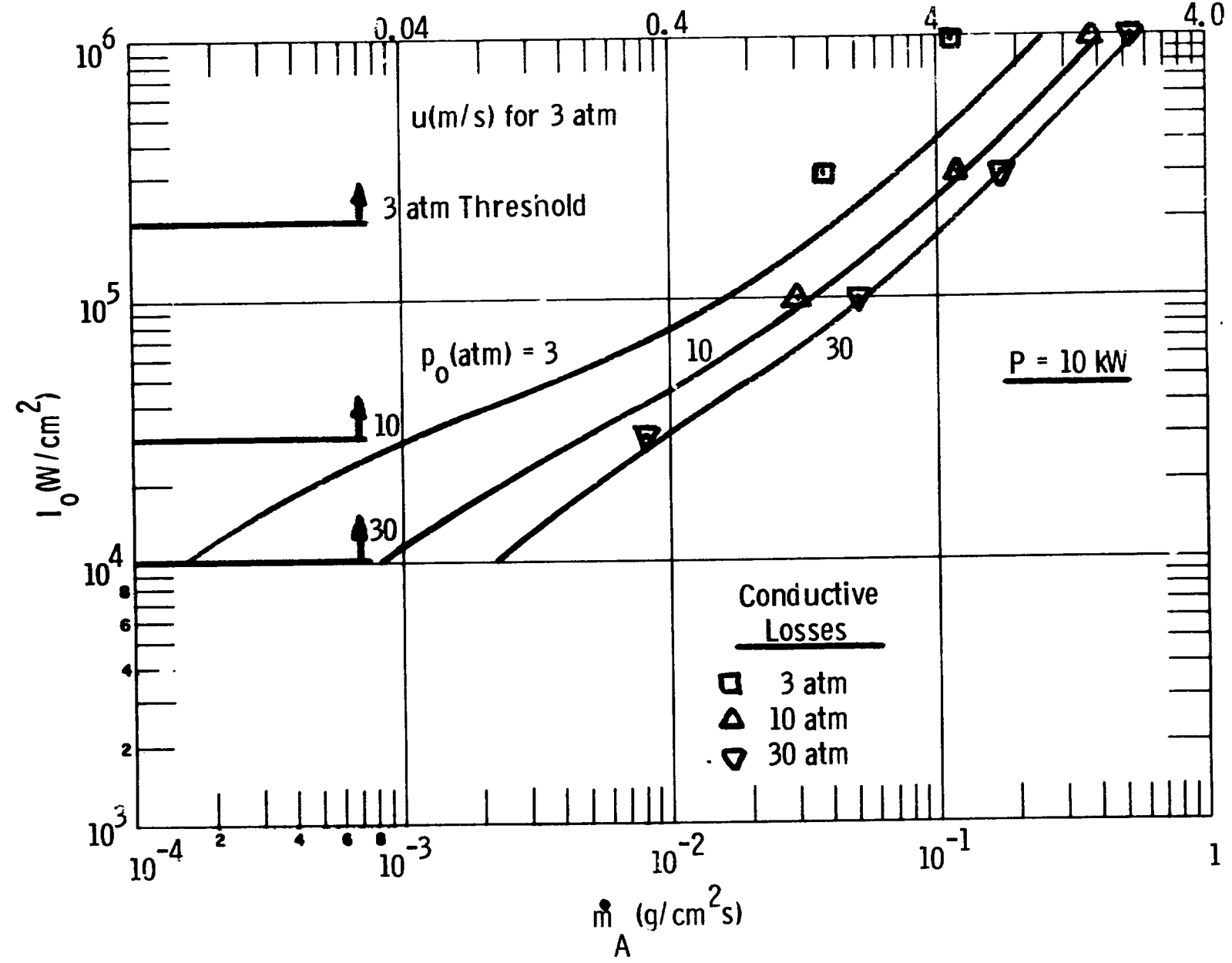

Fig. 4.1b Intensity vs Mass Flow for a Steady LSC Wave with Radial Losses — P = 10 kW.

TABLE 4.1

RESULTS OF LSC WAVE MODEL WITH RADIAL HEAT LOSS

Case	I_o (W/cm^2)	R_i (cm)	T_i (10^3K)	DXMAX (cm)	T_{max} (10^3K)	T_{min} (10^3K)	$\dot{m}_A$ (g/cm^2s)	u_o (cm/s)	% I_o Absorbed
P = 5 MW, p_o = 3 atm, ρ_o = 2.46E-4 g/cm^3, C_3 = 2, C_2 = 0.4, C_{LC} = 3, C_{LR} = 3									
150	1E10	1.26	10	0.1	20.2	18.4	.350	1425	100
151	3E9	2.30	10	0.1	19.0	17.0	.122	497	100
152	1E9	3.99	10	0.1	17.4	15.2	.390	159	100
153	3E8	7.28	10	0.1	15.4	12.8	.00902	36.7	94
154	1E8	12.6	10	0.1	12.9	10.7	.00128	5.20	68
P = 5 MW, p_o = 30 atm, ρ_o = 2.46E-3 g/cm^3, C_3 = 2, C_2 = 0.4, C_{LC} = 3, C_{LR} = 3									
155	1E10	1.26	10	0.01	20.4	19.2	.607	247	100
P = 10 kW, p_o = 3 atm, ρ_o = 2.46E-4 g/cm^3, C_3 = 2, C_2 = 2.4, C_{LC} = 3, C_{LR} = 0									
102	1E10	.0564	10	.05	20.2	15.1	.111	453	90
104	3E9	.103	10	.05	16.9	6.9	.0381	155	80

Case	I_o (W/cm^2)	R_i (cm)	T_i (10^3K)	DXMAX (cm)	T_{max} (10^3K)	T_{min} (10^3K)	$\dot{m}_A$ ($g/cm^2 s$)	u_o (cm/s)	$\%I_o$ Absorbed
P = 10 kW, p_o = 30 atm, ρ_o = 2.46E-3 g/cm^2, C_3 = 1.3, C_2 = 2.4, C_{LC} = 3, C_{LR} = 0									
160	1E10	.0564	10	.01	19.9	17.6	.555	225	100
161	3E9	.103	10	.01	17.9	15.0	.174	70.8	100
162	1E9	.178	8	.01	15.7	10.6	.0503	20.4	96
163	3E8	.326	8	.01	12.6	5.0	.00716	3.24	68
P = 10 kW, p_o = 10 atm, ρ_o = 8.19E-4 g/cm^3, C_3 = 1.3, C_2 = 2.4, C_{LC} = 3, C_{LR} = 0									
140	1E10	.0564	10	.01	20.3	17.3	.377	461	100
141	3E9	.103	10	.01	18.0	14.9	.117	143	99
142	1E9	.178	10	.01	15.9	7.1	.0300	36.6	91

4.2 Beam Convergence

The convergence of the laser beam provides another two-dimensional effect which can change the relation between intensity and mass flux in an LSC wave. If the cross-sectional area of the beam A_B, varies with x, then the intensity I will vary not only because of absorption, but also because of the area change. The conservation of total power in the laser beam requires that IA_B change by absorption, according to

$$\frac{d\, IA_B}{dx} = - k_L\, IA_B \tag{4.4}$$

this is the same relation as (3.5), except here the appropriate area is the beam area A_B instead of the flow area A. The solution is the same as before, namely,

$$IA_B = I_i\, A_{Bi}\, e^{-\tau} \quad , \quad \tau = \int_0^x k_L\, dx \tag{4.5}$$

where the subscript i refers to the location x = 0.

In the one-dimensional model of the wave, we are concerned with conditions near the centerline of the beam, and the laser absorption term in the energy equation is the same as in (2.1) and (2.4), namely,

$$\frac{dI}{dx} = - k_L\, I \tag{4.6}$$

Use of (4.5) then shows this term to be

$$\frac{dI}{dx} = - k_L\, e^{-\tau}\, I_i\, \frac{A_{Bi}}{A_B} \tag{4.7}$$

This shows that the modification required for consideration of beam convergence is to insert the area ratio factor A_{Bi}/A_B in the laser absorption term. This requires some specification ot the beam shape.

A suitable expression for this shape is found for example, in Ref. 10, where the intensity is given as a function of radius r and distance from the focal spot z, as

$$I(r,z) = B\left(\frac{\omega_o^2}{\omega^2}\right)\exp\left(\frac{-2r^2}{\omega^2}\right), \quad \frac{\omega^2}{\omega_o^2} = 1 + \left(\frac{z}{z_o}\right)^2, \quad z_o = \pi\frac{\omega_o^2}{\lambda_L} \qquad (4.8)$$

The shape of the beam is Gaussian in the radial direction, and parabolic along the beam axis, as defined by the function $\omega(z)$. The minimum area is at $z = 0$. There is a size parameter, represented by z_o or ω_o, which also depends on the laser wave length λ_L. A sketch of the shape is shown in Fig. 4.2.

The parameter ω_o is determined by the geometry of the particular lens system used in any given case. Suppose the lens is a distance $z = -L$ from the focal plane, as shown in Fig. 4.2. The corresponding value of ω is denoted as ω_L. At this value of z, (4.8) becomes a quadratic equation for ω_o^2 whose solution is

$$\omega_o^2 = \frac{\omega_L^2}{2}\left[1 - \sqrt{1 - \frac{2L\lambda_L}{\pi\omega_L^2}}^2\right]$$

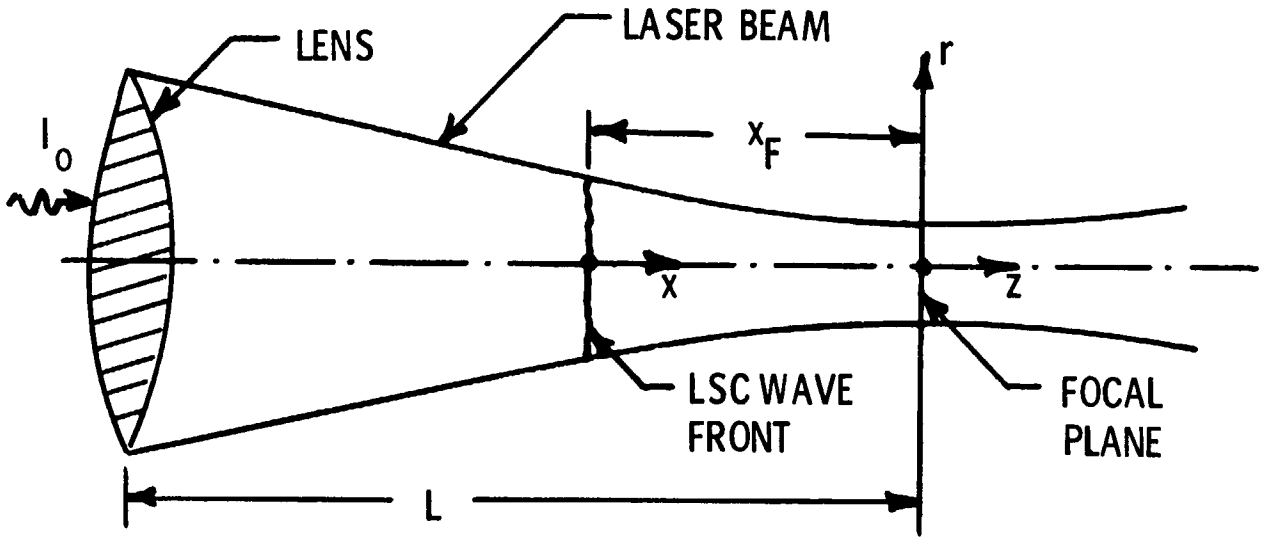

Fig. 4.2 Schematic of Converging Laser Beam

Since the wavelength of interest here is small, 10.6 μm, the radical may be expanded to give

$$\omega_o^2 = \left(\frac{L\lambda_L}{\pi\omega_L}\right)^2 , \quad z_o = \frac{\lambda_L}{\pi}\left(\frac{L}{\omega_L}\right)^2 \tag{4.9}$$

the quantity L/ω_L is the ratio of the distance from the lens to the focal plane to the size of the beam on the lens, which is the f-number of the lens, Thus, the parameter z_o is related to the wavelength and a known property of the lens system.

The beam area can be defined as extending to some fixed point on the Gaussian decay curve, that is to $r/\omega = R_B/\omega$ = constant. Thus R_B^2 is preportional to ω^2. Suppose the beginning of the wave, denoted by subscript i, is at a distance x_F from the focal plane as shown in Fig. 4.2. Then R_{Bi} is at $z = -x_F$, and any other location in the wave is at $z = x - x_F$. The area ratio is then

$$\frac{A_B}{A_{Bi}} = \frac{R_B^2}{R_{Bi}^2} = \frac{z_o^2 + (x-x_F)^2}{z_o^2 + x_F^2} \tag{4.10}$$

This defines the new term in the energy equation in terms of the two physical parameters L/ω_L and x_F. The former is the lens f-number as mentioned above, and the latter is the distance from the focal plane to the wave origin. Notice that the intensity I_i in Eq. (4.7). is the value at $x = 0$, where the wave originates.

With the factor A_{Bi}/A_B inserted in the absorption term on the right of (2.12b), and (4.10) used for this ratio, the LSC wave energy equation may be solved as before, once L/ω_L and x_F are specified. The case of a

constant beam area, considered in Section 2, corresponds to L/ω_L very large compared to x_F, since then (4.10) shows the area ratio to be unity.

As an example of the effect of beam convergence, the calculation of Case 103 was re-done. This is the case of P = 10 kW, p_o = 3 atm, I_i = 3E5 W/cm^2. The value of L/ω_L was taken as 30, which is a high f-number. The value of x_F was estimated by taking the edge of the beam at the e^{-2} level, so that $2R_{Bi}^2/\omega^2(x_F) = 2$. With R_{Bi} determined from the power and intensity by $P = \pi R_{Bi}^2 I_i$, with $\omega(x_F)$ related to z_o by (4.8), and with z_o from (4.9), the value of x_F is 3.075 cm. The LSC wave calculation then gives $\dot{m}_A$ = 0.0845 g/cm^{2}s, u_o = 344 cm/s, compared to 0.0730 and 297 for a parallel beam ($L/\omega_L \to \infty$), Case 103. Thus this rather mildly convergent beam, which has a focal spot radius of 0.01 cm, increases the mass flux by 16%. The location at which 99% of the beam is absorbed is 1.44 cm, well before the focal spot location of x_F = 3.075 cm. The maximum temperature reached is 20,100K, an increase from 19,000K for the parallel beam.

A convergent beam behaves as a higher intensity beam, relative to a parallel beam of the same initial intensity, and necessitates a higher inflow velocity. No other calculations of waves in a converging beam were made. However, they can easily be performed when the geometric parameters L/ω_L and x_F are specified.

A converging beam has the desirable feature of providing static stability for the position of the LSC wave, because of the increase in mass flux with intensity characteristic of LSC waves. If a wave in a convergent beam is displaced upstream to a lower intensity position, the mass flux to keep it steady there will be lower than the mass flux actually occurring, and it will be blown back downstream. If it is displaced downstream to a position of higher intensity, the mass flux required at that position will be higher than that occurring, and it will try to increase the mass flux by moving upstream. In the

divergent portion of the beam, downstream of the focal spot, the same argument shows the wave position to be statically unstable. The question of dynamic stability needs further investigation.

4.3 Transverse Velocity

In the LSC wave experiments done in air, it has been recognized that transverse velocities may be occurring. These experiments are not confined in the radial dimension, so the beam only fills a small part of gas volume. It is then possible for some of the oncoming flow to turn radially and flow around the wave rather than through it. If this actually occurred, it would have the effect of making the experimentally measured wave speeds higher than the ones calculated by a one-dimensional model. This can be seen as follows. (Fig. 4.3) If some of the flow goes around the wave then the streamtube of flow going through the wave has a larger area when it enters the wave than it does far upstream. Thus its axial speed is lower as it enters the wave than it is far upstream. In the one-dimensional model, we calculate the speed as it enters the wave. But the experiments measure the speed far upstream (wave speed relative to the undisturbed flow). Thus the experimental speeds could be higher than the speed of the gas entering the wave.

The measurements made on LSC wave speeds in air do, in fact, show them to be higher than the one-dimensional predictions by about a factor of 3, Ref. 4. They also show evidence of two-dimensional flow, which is consistent with the above explanation. Therefore, in unconfined flows, the one-dimensional predictions of wave speed could be too low because of the neglect of transverse flow effects.

The only attempt made to calculate the effect of transverse velocity on LSC wave structure that is known to the authors is that of Ref. 11, which was quite crude. They estimated that the radial flow might cause the inflow far from the wave to be 1.5 to 2.25 times the value predicted by two-dimensional theory.

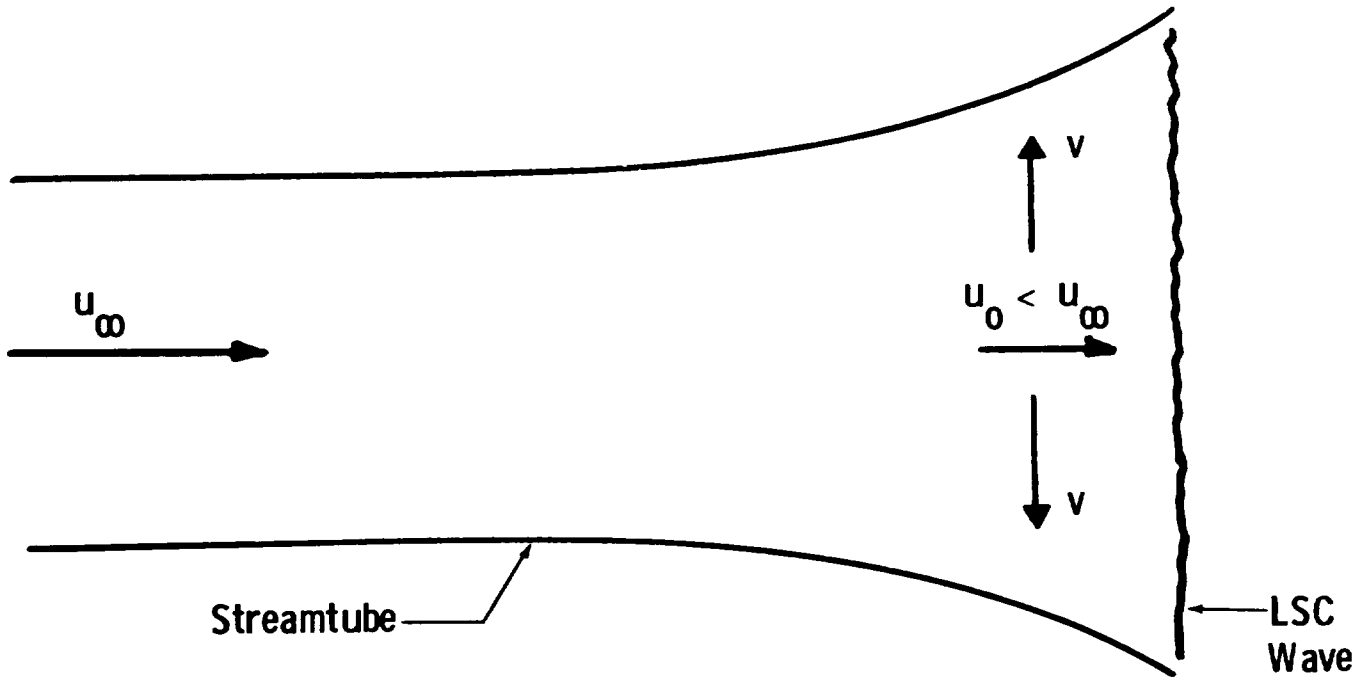

Fig. 4.3 Schematic Diagram of the Effect of Transverse Flow on the Axial Speed of the Incoming Gas Relative to the Wave. Streamtube Divergence causes u_o to be less than u_∞.

In the propulsion application of interest in the present work, the flow occurs in a confined channel, with the laser beam envisioned as heating a major fraction of the gas flow, and with walls bounding the flow in the radial direction. In this case the flow does not have as much freedom to develop radial motion as in the unconfined case. It would appear that the effects of transverse velocity should be much less than in the unconfined case. Unfortunately, no experiments on LSC waves in confined channels have been reported, so empirical evidence for this view is not as yet available.

Considering the difficulty of constructing a model including transverse velocity, and lack of evidence that it is an important factor in confined LSC waves, it was not considered useful within the limited scope of the present work to pursue the subject further.

5. CONCLUSIONS

We have constructed a one-dimensional model of a laser supported combustion (LSC) wave in hydrogen. The pressure in the wave, and the mass flux per unit area, are constants. The temperature profile is determined by the energy conservation equation as a balance between convection, absorption of laser energy, radiation loss to the surroundings, thermal conduction, and radiation transport of energy from the hot part of the wave to the cool part. It has been found that for the conditions of interest the radiation transport may be treated in the radiation conduction approximation.

To obtain the wave structure for a given pressure and laser intensity, a numerical iteration must be performed to find the mass flux. Calculations have been made for pressures of 1, 3, 10 and 30 atm, for 10.6 μm laser intensities from 10^4 to 10^6 W/cm^2. The resulting temperature profiles all show a rapid rise due to heating by conduction and radiation, a high peak due to absorption of laser energy, and a slow decay dominated by radiation losses. The peak temperatures are high because the laser absorption can only occur by inverse bremsstrahlung, and this mechanism requires electrons, which in turn requires high temperatures in hydrogen. At the highest intensities and pressures, the maximum temperature ranges between 20,000 to 30,000K.

The mass flux at each pressure and intensity determines the velocity with which the gas must flow into the wave to keep it stationary. The mass flux increases with pressure at a given intensity. At low intensities the mass flux becomes very small, dropping off toward zero at some threshold value of intensity. This threshold value is strongly affected by transverse losses.

In a laser-heated hydrogen rocket, it is necessary to expand the gas issuing from the LSC wave through a converging-diverging nozzle. The nozzle was modeled by a variable-area, variable-pressure streamtube flow, by adding appropriate terms to the LSC wave energy, mass and momentum conservation equations. A computational scheme was developed for the streamtube flow, using the conditions near the back of the LSC wave as initial conditions. One case was calculated to prove the usefulness of the scheme, and the results compared with a calculation from Ref. 1. In that study, the wave structure was not calculated, so the mass flux to hold the wave stationary was only estimated. The present result showed that the mass flux found by solving the wave structure was nearly a factor of 3 less than that estimated in Ref. 1. This causes the maximum temperature to be much higher than found in Ref. 1 (19,000K rather than 15,000K), which in turn makes the radiation losses much larger. The energy remaining in the gas at the streamtube throat is only 58% of the laser energy, rather than the 95% found in Ref. 1.

The present more complete calculations emphasize the high temperatures and high attendant losses which come from the combination of 10.6 μm laser radiation and hydrogen working fluid. They are caused by reliance on the electron-dependent mechanism of inverse bremsstrahlung for laser energy absorption in a gas where electrons are produced in quantity only above 10,000K. It appears that use of an easily ionizable seedant would be advantageous to permit absorption at lower temperatures and reduce losses.

Several two-dimensional effects were examined. The first was radial heat losses, caused by conductive heat transfer to the surroundings and by black radiation from the edges of the hot gas. Both were modeled approximately to fit into the framework of a one-dimensional model. They are found to be inversely proportional to the cross-sectional area of the hot gas. For the 5 MW power level, these losses have little effect on the mass flux at any given intensity, because this area is large enough to make the radial losses small. However, for the 10 kW power, the small areas produce large

radial losses, which sharply reduce the mass flux from the value it has when these losses are ignored. The results show an effective threshold for the wave which is above 10^6 W/cm^2 for 1 atm, and above 10^4 W/cm^2 at 30 atm, with intermediate values between. This reinforces the view expressed in Ref. 1 that a laser-heated rocket of this type, in a 10 kW size is a loss-dominated device, not scalable to higher powers.

A second two-dimensional effect considered was the convergence of the laser beam, causing an increase in intensity. This was modeled by specifying a laser beam shape in the one-dimensional absorption term. One calculation showed the expected result that the mass flux increased if the beam converged from its initial size at the wave front, instead of remaining parallel. An argument was presented showing that a converging beam leads to static stability of the wave position; dynamic stability was not investigated.

In view of experimental observations of its occurrence in unconfined flows, the question of transverse flow was addressed briefly. It is speculated that transverse flows cause the large observed deviations of mass flow from one-dimensional theoretical values. However, the propulsion applications envisioned as the motivation for the present work will involve flows which are confined radially. Therefore, transverse flow is expected to be less severe than in radially unconfined flows, although there are no experiments in such flows to verify this assertion. Considering this uncertainty of the importance of transverse flow in propulsion applications, and the difficulty of estimating such effects theoretically, no further work on this subject was undertaken in the present study.

REFERENCES

1. Kemp, N. H., Root, R. G., Wu, P. K. S., Caledonia, G. E. and Pirri, A. M., "Laser-Heated Rocket Studies" NASA CR-135127 (PSI TR-53), Physical Sciences Inc., Woburn, MA, May 1976.

2. Raizer, Yu. P., "Subsonic Propagation of a Light Spark and Threshold Conditions for the Maintenance of Plasma by Radiation", Soviet Physics JETP, Vol. 31, No. 6, December 1970, pp. 1148 - 1154.

3. Boni, A. A. and Su, F. Y., "Propagation of Laser Supported Deflagration Waves", Physics of Fluids, Vol. 17, No. 2, February 1974, pp. 340 - 342.

4. Jackson, J. P. and Nielsen, P. E., "Role of Radiative Transport in the Propagation of Laser Supported Combustion Waves", AIAA Journal, Vol. 12, No. 11, November 1974, pp. 1498 - 1501.

5. Boni, A. A. and Su, F. Y., "Subsonic Propagation of Laser Supported Waves", AIAA Paper No. 74-567, 1974.

6. Su, F. Y. and Boni, A. A., "Nonlinear Model of Laser Supported Deflagration Waves", Physics of Fluids, Vol. 19, No. 7, July 1976, pp. 960 - 966.

7. Pirri, A. N., Kemp, N. H., Root, R. G. and Wu, P. K. S., "Theoretical Laser Effects Study", Final Report to Naval Research Laboratory on Contracts N00014-74-C-0207 and N00172-76-C-0216 (PSI TR-89), Physical Sciences Inc., Woburn, MA, Feburary 1977.

8. Klosterman, E. L. and Byron, S. R., "Measurement of Subsonic Laser Absorption Wave Propagation Characteristics at 10.6 μm", Journal of Applied Physics, Vol. 45, No. 11, November 1974, pp. 4751 - 4759.

9. Fowler, M. C. and Smith, D. C., "Ignition and Maintenance of Subsonic Plasma Waves in Atmospheric Pressure Air by CW CO_2 Laser Radiation and Their Effects on Laser Beam Propagation", Journal of Applied Physics, Vol. 46, No. 1, January 1975, pp. 133 - 150.

10. Yariv, A., "Quantum Electronic," John Wiley and Sons, New York, 1968, p. 224.

11. Thomas, P. D., Musual, H. M. and Chou, Y. S., "Laser Beam Interaction – Part II", Final Technical Report to Army Missile Command under contract DAAH01-74-C-0278 (LMSC-D403747), Lockheed Missiles and Space Company, Inc., Palo Alto, CA, August 1974.

APPENDIX A

THERMODYNAMIC PROPERTIES OF EQUILIBRIUM HYDROGEN

We need the derivatives of enthalpy with respect to p and T, the equation of state which relates ρ and T, and the composition of the mixture of hydrogen molecules, atoms, ions and electrons. The pressure derivative of h can be expressed in terms of the equation of state by a classical use of reciprocity relations between the derivatives of h and entropy, which are in turn obtained from the second law. These lead to

$$\rho \left(\frac{\partial h}{\partial p} \right)_T = \left(\frac{\partial \ln \rho}{\partial \ln T} \right)_p + 1 \qquad \text{(A-1)}$$

We characterize the hydrogen as a mixture of perfect gases whose components have number densities: molecules n_M, atoms n_A, ions n_I and electrons n_E. We do not expect to get a temperature where other species are significant, nor are there multiply ionized atoms, so $n_I = n_E$. As reaction coordinates we use the fraction of molecules dissociated β and the fraction of atoms ionized, α:

$$\beta = \frac{(n_A + n_I)/2}{n_M + (n_A + n_I)/2} \quad , \quad \alpha = \frac{n_I}{n_A + n_I} \qquad \text{(A-2)}$$

In terms of the original number of particles per unit volume,

$$n_o = n_M + (n_A + n_I)/2 \qquad \text{(A-3)}$$

the number density of the species are

$$n_M = n_o (1 - \beta), \quad n_A = 2 n_o \beta (1 - \alpha), \quad n_I = n_E = 2 n_o \beta \alpha \quad (A-4)$$

and the corresponding partial pressure are found from

$$p_i = n_i kT \quad (A-5)$$

where k is the Boltzmann constant. The partial mass densities are, in terms of the particle masses m_i,

$$\rho_M = n_M m_M, \ \rho_A = n_A m_A, \ \rho_I = n_I m_I, \ \rho_E = n_I m_E \quad (A-6)$$

and the total number and mass densities are

$$n = n_o [1 + 9 (1 + 2\alpha)], \ \rho = n_o m_M \quad (A-7)$$

Whenever convenient we will use the facts that an excellent approximation for hydrogen is $m_A = m_I = m_M/2$.

The equation of state is the sum of the partial pressures,

$$p = \rho Z R_M T, \quad Z = 1 + \beta (1 + 2\alpha), \quad R_M = k/m_M$$

$$(\partial \ln \rho / \partial \ln T)_p = - 1 - (\partial \ln Z / \partial \ln T)_p \quad (A-8)$$

where Z is the compressibility factor and R_M the gas constant for the molecules. We have now expressed ρ in terms of p, T through α and β by (A-8). Since p and T are the dependent variables, we need α, β in terms of T, p.

Since we deal with hydrogen in thermochemical equilibrium, α and β are determined by the Law of Mass Action in terms of the thermodynamic variables of the mixture. There are two reactions occuring, dissociation and ionization:

$$H_2 \rightleftarrows 2H \qquad H \rightleftarrows H^+ + E^-$$

For each the equilibrium constant provides a relation between the partial pressures and the partition functions of the species, involving the heat of reaction. These relations are

$$\frac{p_A^{\,2}}{p_M} = \left(\frac{\pi m_A}{h_P^{\,2}}\right)^{3/2} \frac{(kT)^{5/2} Q_{elA}^{\,2}}{Q_c Q_v Q_r Q_{elM}} e^{-h_D^{\,o} m_M/kT} \qquad \text{(A-9a)}$$

$$\frac{p_I p_E}{p_A} = \left(\frac{2\pi m_E}{h_P^{\,2}}\right)^{3/2} (kT)^{5/2} \frac{Q_{elI} Q_{elE}}{Q_{elA}} e^{-h_{IL}^{\,o} m_I/kT} \qquad \text{(A-9b)}$$

where h_P is Planck's constant, Q_v and Q_r are the vibrational and rotational partition functions of H_2, Q_c is a partition function reflecting vibration-rotation coupling, Q_{eli} are the electronic partition functions of the species, $h_D^{\,o}$ is the heat of dissociation of a molecule per unit mass and $h_{IL}^{\,o}$ is the heat of ionization of an atom per unit mass. From (A-4), (A-5), (A-7) and (A-8) the partial pressure/ratios are

$$\frac{p_A^{\,2}}{p_M} = \frac{4\beta^2 (1-\alpha)^2}{1-\beta} n_o kT = \frac{4\beta^2 (1-\alpha)^2}{1-\beta} \frac{p}{Z} \qquad \text{(A-10a)}$$

$$\frac{p_I p_E}{p_A} = \frac{4\beta^2 \alpha^2}{2\beta (1-\alpha)} n_o kT = \frac{2\beta \alpha^2}{1-\alpha} \frac{p}{Z} \qquad \text{(A-10b)}$$

The electronic partition function for the molecule may be replaced by its ground-state statistical weight 1, since its first excited state lies very high (132,000 K). For the electron $Q_{elE} = 2$ because of the two electron spin states, and for the ion, there are no internal states, $Q_{elI} = 1$.

Using (A-10) in (A-9), with Z from (A-8), yields

$$\frac{\beta^2 (1 - \alpha)^2}{(1 - \beta)[1 + \beta(1 + 2\alpha)]} = \frac{f_D(T)}{p} \qquad \text{(A-11a)}$$

$$\frac{\beta \alpha^2}{(1 - \alpha)[1 + \beta(1 + 2\alpha)]} = \frac{f_I(T)}{p} \qquad \text{(A-11b)}$$

where we have defined

$$f_D = \frac{T^{5/2} e^{-\theta_D/T}}{Q_c Q_r Q_v} \frac{Q_{elA}^2}{4} k \left(\frac{\pi m_A k}{h_P^2} \right)^{3/2}, \quad \theta_D = h_D^{\circ} m_M / k \qquad \text{(A-12a)}$$

$$= 51,970 \text{ K}$$

$$f_I = \frac{T^{5/2} e^{-\theta_{IL}/T}}{Q_{elA}} k \left(\frac{2\pi m_E k}{h_P^2} \right)^{3/2}, \quad \theta_{IL} = h_{IL}^{\circ} m_I / k \qquad \text{(A-12b)}$$

Equations (A-11) define α, β in terms of p, T, and could be used. However, they are difficult to solve for α and β, and can be simplified considerably for hydrogen without much loss of accuracy. Equilibrium hydrogen dissociates almost completely before it ionizes significantly. We can thus separate the two reactions, and assume α is small during dissociation, while β goes from 0 to 1. Then β is near unity while α increases from near zero. These two approximations are separated by a temperature T^*

below which there are molcules and atoms with very few electrons, and above which there are atoms, ions and electrons, with few molecules. Therefore we use

$$T < T^*: \quad \frac{\beta^2}{1-\beta^2} = \frac{f_D(T)}{p}, \quad \frac{\beta\,\alpha^2}{1+\beta} = \frac{f_I(T)}{p} \tag{A-13a}$$

$$T > T^*: \quad \frac{(1-\alpha)^2}{2(1-\beta)(1+\alpha)} = \frac{f_D(T)}{p}, \quad \frac{\alpha^2}{2(1-\alpha^2)} = \frac{f_I(T)}{p} \tag{A-13b}$$

There are easily solved for β and α to yield

$$T < T^*: \ \beta = (1 + p/f_D)^{-/2}, \ \alpha = \left[\frac{1+\beta}{\beta}\ \frac{f_I}{p}\right]^{1/2} \tag{A-14a}$$

$$T > T^*: \ \alpha = (1 + p/2f_I)^{-1/2}, \ 1 - \beta = \frac{(1-\alpha)^2}{1+\alpha}\ \frac{p}{2f_D} \tag{A-14b}$$

In general we will only use β as variable below T^* from (A-14a), and take $\alpha = 0$. Above T^* we will take α as variable, and $\beta = 1$. The second expressions in Eqs. (A-14) will only be used if an estimate is needed for α below T^* which differs from zero, or for β above T^* which differs from unity.

To complete the specification of f_D and f_I we need the partition functions. The combination $Q_c\,Q_r\,Q_v$ can be found in Ref. A1, p. 163, Eq. (7.39), where it is called Q_{vjm}. It may be divided as follows:

$$Q_r = T/2\,\theta_r, \quad Q_v = \left(1 - e^{-\theta_v/T}\right)^{-1} \tag{A-15}$$

The factor 2 in Q_r has been added to Ref. A1 because of the symmetry of the hydrogen molecule. The vibrational and rotational temperature constants θ_v and θ_r come from Eqs. (7.32) and (7.33), p. 162, of Ref. A1 using the JANNAF spectroscopic constants (in cgs units)

$$B_e = 60.848, \quad \omega_e = 4405.3, \quad x_e = 125.325/4405.3 = .0284$$

$$\delta = 3.0664/60.848 = .0504, \quad \gamma = 60.848/4405.3 = .0138$$

They are

$$\theta_v = \frac{h_P c \omega_e (1 - 2x_e)}{k}, \quad \theta_r = \frac{h_P c B_e}{k} \left(1 - \frac{\delta}{2}\right)$$

$$\theta_v = 5978 \text{ K} \qquad \theta_r = 85.34 \text{ K}$$

The remaining factor Q_c is the coupling partition function,

$$Q_c = 1 + \frac{\theta_r}{3T} + \frac{8\gamma^2 T}{\theta_r} + \frac{\delta}{e^{\theta_v/T} - 1} + \frac{2 x_e \theta_v/T}{\left(e^{\theta_v/T} - 1\right)^2} \qquad \text{(A-16)}$$

$$= 1 + \frac{28.45}{T} + 1.785 \times 10^{-5} T + \frac{5.04 \times 10^{-2}}{e^{\theta_v/T} - 1} + \frac{5.68 \times 10^{-2} \theta_v/T}{\left(e^{\theta_v/T} - 1\right)^2}$$

The last expression needed is for the electronic partition function of the atoms, which is

$$Q_{elA} = 2S_1 e^{-\theta_{IL}/T}, \quad S_1 = \sum_{j=1}^{L} j^2 e^{\theta_{IL}/T\, j^2} \qquad \text{(A-17)}$$

The first term is the ground state weight 2. The subsequent terms account for excited electronic states. The upper limit of the sum must be finite, since the terms grow like j^2 for large j. The finite cut-off means that above some degree of excitation the electron is no longer considered bound to an atom, but is a free electron. Related to this necessity for cutting off the sum is the lowering of the ionization potential. The value of h_{JL}^{o} is not that for removing an electron <u>infinitely</u> far from an atom, because in an ionized mixture the electron no longer is considered bound when it is far enough from the atom to be indistinguishable from other electrons. Thus θ_{IL} is not the value θ_I = 157,770 K obtained from the spectroscopic constants for a very weakly ionized mixture, but a lower value (hence the subscript L). If these two effects are not accounted for, the composition of equilibrium hydrogen at high temperatures and pressure will be noticably in error, as found in Ref. A2, Table 7.1.

The lowering of the ionization potential is discussed in Ref. A3. In Eq. (3.85), p. 218, it is suggested that

$$\Delta I = k \Delta \theta_I = 2 e^3 (2\pi n_E/kT)^{1/2}$$

where e is the charge in esu, and the other units are cgs. For hydrogen, $e = 4.803 \times 10^{-10}$ esu, and we have

$$\Delta I = 4.728 \times 10^{-20} \left[\frac{n_E\,(cm^{-3})}{T(K)} \right]^{1/2} \text{ ergs}$$

$$= 4.728 \times 10^{-30} \left[\frac{n_E\,(m^{-3})}{T(K)} \right]^{1/2} \text{ Joules} \qquad \text{(A-18)}$$

This relates the lowering of the ionization potential to T and the electron density, which is in turn related to α by Eq. (A-4), and so depends on θ_{IL} through f_I in Eq. (A-14b). Thus the determination of α is an iterative process, requiring iteration on θ_{IL}. It also requires iteration on the upper limit L of the sum in Eq. (A-17), which is related to θ_{IL}. There are a number of such relations which can be used. Here we have chosen a simple one, namely to cut off when

$$\theta_I/j^2 > \Delta I/k \ .$$

In the present work we have used one step in the iteration, calculating α by the following procedure:

1) Find α from Eq. (A-14a) using $\theta_{IL} = \theta_I = 157,770$ K, L = 17.
2) Find n_E from Eqs. (A-4) and (A-7) using this α.
3) Find ΔI from Eq. (A-18).
4) Calculate $\theta_{IL} = \theta_I - \Delta I/1.3806 \times 10^{-22}$.
5) Calculate a cut-off L = greatest integer in $[\theta_I/(\theta_I - \theta_{IL})]^{1/2}$.
6) Recalculate α using θ_{IL} and this L.

The resulting value of α is taken as the correct one. Further iterations could be performed, but it will be seen that this one iteration yields quite accurate results.

This calculation of Q_{elA} is used only for $T > T^*$, where α is the varying reaction coordinate and $\beta = 1$ in general. (However, if an estimate of β different from unity is needed, we may use this Q_{elA} in the second of Eqs. (A-14b).) For $T < T^*$, there is very little ionization and the temperature is low, so we may take $Q_{elA} = 2$, its ground state value, to calculate the varying reaction coordinate β. The value of α in this region is zero. (If an estimate of α different from zero is needed, we may use the second of Eqs. (A-14a), with $Q_{elA} = 2$.)

The derivatives of α and β are needed for the wave and nozzle computations. From Eqs. (A-14) it is easy to find them. In the appropriate temperature ranges we have:

$$\left(\frac{\partial \beta}{\partial T}\right)_p = \frac{\beta(1-\beta^2)}{2} \frac{d \ln f_D}{dT}, \left(\frac{\partial \alpha}{\partial T}\right)_p = \frac{\alpha(1-\alpha^2)}{2} \frac{d \ln f_I}{dT}$$

In the differentiation of f_D, the complicated expression of $d \ln Q_c/dT$ is ignored as a small correction, its value taken to be unity. (The value of specific heat so derived are shown later to be quite accurate.) Only Q_r and Q_v have to be differentiated. The result is

$$T < T^*: \left(\frac{\partial \beta}{\partial \ln T}\right)_p = \frac{\beta(1-\beta^2)}{2}\left[\frac{3}{2} + \frac{\theta_D}{T} - \psi_v\right] \qquad \text{(A-19a)}$$

$$\psi_v = \frac{\theta_v/T}{e^{\theta_v/T} - 1}, \quad \left(\frac{\partial \alpha}{\partial T}\right)_p = 0$$

$$Z = 1 + \beta, \qquad \left(\frac{\partial \ln Z}{\partial \ln T}\right)_p = \frac{1}{1+\beta}\left(\frac{\partial \beta}{\partial \ln T}\right)_p$$

A similar differentiation of f_I involves only the factors $T^{5/2}$ and S_1, since the $\exp(-\theta_{IL}/T)$ factor cancels with the one in Q_{elA}. The result is

$$T > T^*: \left(\frac{\partial \alpha}{\partial \ln T}\right)_p = \frac{\alpha(1-\alpha^2)}{2}\left[\frac{5}{2} + \frac{\theta_{IL}}{T}\frac{S_2}{S_1}\right] \qquad \text{(A-19b)}$$

$$S_2 = \sum_{j=1}^{L} \exp(\theta_{IL}/T\, j^2) = -\frac{T^2}{\theta_{IL}} \frac{dS_1}{dT}, \quad \left(\frac{\partial \beta}{\partial T}\right)_p = 0$$

$$Z = 2(1+\alpha), \qquad \left(\frac{\partial \ln Z}{\partial \ln T}\right)_p = \frac{1}{1+\alpha}\left(\frac{\partial \alpha}{\partial \ln T}\right)_p$$

The derivatives with respect to p are even similar, since f_D and f_I are only functions of T.

$$T < T^*: \left(\frac{\partial \alpha}{\partial p}\right)_T = 0, \quad \left(\frac{\partial \beta}{\partial p}\right)_T = -\frac{\beta(1-\beta^2)}{2p}$$

$$Z = 1 + \beta, \qquad \left(\frac{\partial \ln Z}{\partial \ln p}\right)_T = -\frac{\beta(1-\beta)}{2} \tag{A-20a}$$

$$T > T^*: \left(\frac{\partial \beta}{\partial p}\right)_T = 0, \quad \left(\frac{\partial \alpha}{\partial p}\right)_T = -\frac{\alpha(1-\alpha^2)}{2p}$$

$$Z = 2(1+\alpha), \qquad \left(\frac{\partial \ln Z}{\partial \ln p}\right)_T = -\frac{\alpha(1-\alpha)}{2} \tag{A-20b}$$

The remaining thermodynamic properties needed are the enthalpy, and the specific heat c_p. The enthalpy is found by summing the contributions of the various components. The translational specific heats of the atoms, ions and electrons are 5k/2 per particle. For the ions and electrons, this is the total specific heat, so their values per unit mass are

$$c_{pI} = 5k/2m_I, \quad c_{pE} = 5k/2m_E = c_{pI}\, m_I/m_E \tag{A-21}$$

The corresponding enthalpies are the integrals with respect to T. In addition the ions carry the dissociation energy h_D^o and the ionization energy h_{IL}^o. Therefore

$$h_E = c_{pE}\, T, \quad h_I = c_{pI}\, T + h_D^o + h_{IL}^o \tag{A-22}$$

The atoms have a translational contribution $5\,kT/m_A$, carry the dissociation energy h_D^o and also have a contribution from the electronic states derived from Q_{elA} of Eq. (A-17) by

$$h_{elA} = \frac{kT^2}{m_A} \frac{\partial \ln Q_{elA}}{\partial T} = h_{IL}^o \left(1 - \frac{S_2}{S_1}\right)$$

where S_2 has been defined in Eq. (A-19b). Thus the atomic enthalpy is

$$h_A = \frac{5\,kT}{2\,m_A} + h_D^o + h_{IL}^o \left(1 - \frac{S_2}{S_1}\right) \qquad \text{(A-23)}$$

Finally, the molecules have a translational contribution $5\,kT/2m_M$ from the two rotational degrees of freedom corresponding to $Q_r = T/2\theta_r$, and a vibrational contribution found from Q_v by

$$h_v = \frac{kT^2}{m_M} \frac{\partial \ln Q_v}{\partial T} = \frac{kT}{m_M} \psi_v$$

where ψ_v has been defined in Eq. (A-19a). Thus the molecular enthalpy is

$$h_M = \frac{kT}{m_M} \left(\frac{7}{2} + \psi_v\right) \qquad \text{(A-24)}$$

The enthalpy of the mixture is the sum of the species enthalpies, weighted by their mass fractions:

$$h = \sum h_i \rho_i / \rho \qquad \text{(A-25)}$$

The mass fractions are found in terms of α and β by using Eqs. (A-4), (A-6) and (A-7):

$$\frac{\rho_M}{\rho} = 1 - \beta, \quad \frac{\rho_A}{\rho} = \beta\,(1 - \alpha), \quad \frac{\rho_I}{\rho} = \beta\,\alpha, \quad \frac{\rho_E}{\rho} = \frac{\beta\,\alpha\,m_E}{m_I} \qquad (A-26)$$

In the low temperature region there are only molecules and atoms, we use $h = h_M\,\rho_M/\rho + h_A\,\rho_A/\rho$ with $\alpha = 0$. In h_A we ignore the last term since the first terms of S_2 and S_1 are equal. We then find from Eqs. (A-23), (A-24) and (A-26):

$$T < T^*: \quad h = \frac{5\,kT}{2\,m_A}\,[(0.7 + 0.2\,\psi_v)\,(1 - \beta) + \beta\,(1 + 0.2\,\theta_D/T)] \qquad (A-27a)$$

In the high temperature region there are atoms, ions and electrons, but $\beta = 1$. Then Eqs. (A-22), (A-23), (A-25) and (A-26) yield

$$T > T^*: \quad h = \frac{5\,kT}{2\,m_A}\left\{1 + \alpha + \frac{0.2\,\theta_D}{T} + \frac{0.4\,\theta_I}{T}\left[1 - (1 - \alpha)\,\frac{S_2}{S_1}\right]\right\} \qquad (A-27b)$$

The equilibrium specific heat is obtained by differentiation at constant pressure. Two new functions of T enter from the derivatives of ψ_v and S_2. They are

$$\phi_v = \psi_v^2\, e^{\theta_v/T} = T\,d\psi_v/dT + \psi_v$$

$$S_4 = \sum_{j=1}^{L} j^{-2} \exp(\theta_{IL}/T\,j^2) = -\,(T^2/\theta_{IL})\,d\,S_2/dT \qquad (A-28)$$

With those, and dS_1/dT from Eq. (A-19b), the derivatives of (A-27) are

$$T < T^*: \quad c_p = \frac{5k}{2m_A} \left[(1-\beta)(0.7 + 0.2\,\Phi_v) + \beta + T\left(\frac{\partial \beta}{\partial T}\right)_p \left(0.3 + 0.2\,\frac{\theta_D}{T} - 0.2\,\psi_v\right)\right] \quad \text{(A-29a)}$$

$$T > T^*: \quad c_p = \frac{5k}{2m_A} \left[1 + \alpha + 0.4\,\frac{\theta_{IL}}{T}\,(1-\alpha)\left(\frac{S_4}{S_1} - \frac{S_2^{\,2}}{S_1^{\,2}}\right) + T\left(\frac{\partial \alpha}{\partial T}\right)_p \left(1 + 0.4\,\frac{\theta_{IL}}{T}\,\frac{S_2}{S_1}\right)\right] \quad \text{(A-29b)}$$

There remains only the specification of T^*, the temperature at which we shift from dissociation with no ionization to ionization with full dissociation. Probably the most accurate compilation of the properties of equilibrium hydrogen is that of Patch, Ref. A7. A perusal of his tables shows that the first temperature at which the number of hydrogen molecules is less than the number of electrons is given by the following table:

p (atm):	1	3	10	30	100
T (10^3K):	7.3	8	9	10	11

If we take these values as T^*, except using 7000 instead of 7300 at 1 atm, then the relation

$$T^* = 2000 \log_{10} p(\text{atm}) + 7000 \quad \text{(A-30)}$$

fits p = 1, 10, and 100, and is very close to the values at p = 3, 30. We will adopt Eq. (A-30) as the definition of T^*.

A comparison of some values calculated using the expressions given in this Appendix with those given by Patch is shown in Table A1. The enthalpies from Patch have had 2.16×10^8 J/kg added to them because of his use of the atom as the zero of enthalpy, rather than the molecule which is used here.

The comparison shows the present properties to be an excellent approximation to those resulting from Patch's elaborate calculations. The major species are in agreement within a few percent, as are the enthalpies and the specific heats. Only the minor species have serious differences, that is, electrons below T^* and molecules above T^*. It should be noted that Patch has included H_2^+, H_3^+, H^- which are not considered here. He also distinguishes the ground electronic state and excited electronic states of both H_2 ($H_2^\ddagger$ and H_2^*) and H ($H^\ddagger$, H^*). We have added these in our comparison. He also has two cut-offs for Q_{elA}; one is that used here, the other a distance cut-off. His values of c_p were obtained by numerical differentiation of h.

Considering the relative simplicity of the present model, it provides excellent accuracy for the thermodynamic properties of equilibrium hydrogen.

Although it is not used in the integration, the Mach number is an interesting parameter which can be calculated when p and T are known, since they determine the speed of sound a. For a gas in thermochemical equilibrium, the second law of thermodynamics and the expression of h as a function of ρ and p shows that

$$a^2 \equiv \left(\frac{\partial p}{\partial \rho}\right)_s = \frac{(\partial h/\partial \rho)_p}{\rho^{-1} - (\partial h/\partial p)_\rho}$$

Conversion of these derivatives to h as a function of T and p, and use of (A-1) shows that

$$a^2 = \left[\left(\frac{\partial \rho}{\partial p}\right)_T - \frac{1}{c_p T}\left(\frac{\partial \ln \rho}{\partial T}\right)_p^2\right]^{-1}$$

The second derivative has already been expressed in terms of Z by (A-8). From the gas law (A-8) it is also easy to see that

$$\left(\frac{\partial \rho}{\partial p}\right)_T = \frac{1}{R_M Z T}\left[1 - \left(\frac{\partial \ln Z}{\partial \ln p}\right)_T\right]$$

Thus the Mach number squared is

$$M^2 = \frac{u^2}{a^2} = \frac{u^2}{T}\left\{\frac{1}{R_M Z}\left[1 - \left(\frac{\partial \ln Z}{\partial \ln p}\right)_T\right] - \frac{1}{c_p}\left[1 + \left(\frac{\partial \ln Z}{\partial \ln T}\right)_p\right]^2\right\} \quad \text{(A-31)}$$

The T derivative of Z is given in (A-19), and the p derivatives are given in (A-20). Thus the Mach number can be calculated as the integration progresses.

TABLE A1

COMPARISON OF PRESENT THERMODYNAMIC PROPERTIES WITH PATCH (Ref. A4)

T (10^3K)	n_M (m^{-3})		n_A (m^{-3})		n_E (m^{-3})		h (J/kg)		c_p (J/kg K)	
	PSI	P	PSI	P	PSI	P	PSI	P	PSI	P
					p 1 atm					
4	4.27^{23}	4.28^{23}	1.41^{24}	1.40^{24}	7.99^{16}	8.84^{16}	2.09^{8}	2.12^{8}	17.6^{4}	17.3^{4}
8	3.15^{20}	3.36^{20}	9.13^{23}	9.13^{24}	2.09^{21}	2.09^{21}	3.84^{8}	3.84^{8}	2.55^{4}	2.55^{4}
12	1.30^{19}	1.44^{16}	4.97^{23}	4.98^{23}	5.71^{22}	5.72^{22}	6.25^{8}	6.24^{8}	12.80^{4}	12.71^{4}
16	2.55^{17}	2.10^{17}	1.13^{23}	1.15^{23}	1.73^{23}	1.74^{23}	15.5^{8}	15.4^{8}	27.0^{4}	25.9^{4}
20	1.75^{15}	3.47^{15}	1.50^{22}	1.50^{22}	1.76^{23}	1.78^{23}	22.3^{8}	22.2^{8}	8.86^{4}	8.88^{4}
					p = 10 atm					
4	1.12^{25}	1.12^{25}	7.20^{24}	7.18^{24}	1.81^{17}	4.65^{17}	1.22^{8}	1.25^{8}	11.2^{4}	11.1^{4}
8	3.15^{22}	3.36^{22}	9.13^{24}	9.13^{24}	6.55^{21}	6.67^{21}	3.79^{8}	3.80^{8}	2.22^{4}	2.36^{4}
12	1.72^{21}	1.90^{21}	5.72^{24}	5.72^{24}	1.99^{23}	1.99^{23}	5.16^{8}	5.16^{8}	5.64^{4}	5.61^{4}
16	1.60^{20}	1.81^{20}	2.78^{24}	2.81^{24}	9.01^{23}	9.11^{23}	9.58^{8}	9.51^{8}	17.3^{4}	17.1^{4}
20	6.70^{18}	8.54^{18}	7.77^{23}	7.92^{23}	1.45^{24}	1.48^{24}	17.7^{8}	17.5^{8}	19.0^{4}	19.0^{4}
					p = 100 atm					
4	1.56^{26}	1.57^{26}	2.70^{25}	2.69^{25}	3.50^{17}	3.01^{18}	$.84^{8}$	$.87^{8}$	5.03^{4}	5.09^{4}
8	2.97^{24}	3.16^{24}	8.87^{25}	8.85^{25}	2.04^{22}	2.18^{22}	3.65^{8}	3.66^{8}	3.32^{4}	3.32^{4}
12	1.89^{23}	2.07^{23}	5.96^{25}	5.96^{25}	6.71^{23}	6.75^{23}	4.81^{8}	4.79^{8}	3.29^{4}	3.32^{4}
16	3.14^{22}	3.35^{22}	3.86^{25}	3.88^{25}	3.62^{24}	3.68^{24}	6.92^{8}	6.90^{8}	7.80^{4}	7.79^{4}
20	4.93^{21}	5.51^{20}	2.04^{25}	2.06^{25}	8.16^{24}	8.53^{24}	11.5^{8}	11.3^{8}	14.3^{4}	14.1^{4}

APPENDIX B

ABSORPTION OF LASER ENERGY

The absorption of the incident laser energy by the plasma is dependent on k_L, the absorption coefficient of the plasma. Based on the studies of Ref. A5, we use as the absorption mechanism inverse Bremsstrahlung, both electron-ion and electron-neutral. The expressions for k_L have been given in Ref. A5. The electron-ion absorption is given in Eq. (2.1) there as

$$k_{LEI} = \sigma_{EI}\, n_E\, n_I\, [\exp(h_P\, \nu/kT) - 1]$$

σ_{EI} is the electron-ion absorption cross-section and ν is the laser frequency (for 10.6 μm in the present case). The cross-section is given in Eq. (2.2) of Ref. A5 as

$$\sigma_{EI} = \frac{4}{3}\left(\frac{2\pi}{3 m_E kT}\right)^{1/2} \frac{Z^2 e^6}{h_P c m_E \nu^3} = \frac{1.63 \times 10^{-32}}{T^{1/2}}\ (\mathrm{cm}^5)$$

where Ze is the ion charge, e is the electron charge and c is the speed of light. Combining these two equations we find

$$k_{LEI} = \frac{1.63 \times 10^{-32}}{T^{1/2}}\, n_E\, n_I\, (e^{1357/T} - 1)\ (\mathrm{cm}^{-1})$$

where T is in K and n_E, n_I are in cm^{-3}.

The electron and ion number densities are related to the pressure by Eqs. (A-6), (A-7) and (A-8) as

$$n_E = n_I = 2 \alpha \beta p / kT Z \qquad (B-1)$$

The above expression for k_{LEI} is a semi-classical result. To account for quantum - mechanical effects we multiply by a Gaunt factor of 1.5, which is an average value for the range of interest. The final expression for the electron-ion inverse Bremsstrahlung absorption coefficient is then

$$k_{LEI} = 5.1 \times 10^{a} \frac{\alpha^2 \beta^2 p^2}{T^{5/2} Z^2} (e^{1357/T} - 1) \qquad (B-2)$$

a = 0 for cgs units, a = 4 for mks units.

Of course, this expression is only valid where there are ions, $\alpha \neq 0$, so in our approximation for the chemistry, it is to be used only above T^*, where $\beta = 1$.

The absorption coefficient for electron-neutral inverse Bremsstrahlung is also given in Ref. A5, Eq. (2.6), as

$$k_{LEN} = Q_{EN} n_E n_N [1 - \exp(-h_P \nu / kT)]$$

where Q_{EN} is the absorption cross-section and n_N is the neutral number density. Equation (2.8) of Ref. A5 gives

$$Q_{EN} = \frac{2.96 \times 10^{-45} T}{1 - \exp(-h_P \nu / kT)} \left(\frac{h_I^{\circ} m_I}{h_P \nu} \right)^2 e^{-\xi \left(\frac{m_I h_I^{\circ}}{kT} \right)^{1/2}} \quad (cm^5)$$

where ξ may be approximated by the first two terms of Eq. (2.9) of Ref. A5, when $\sqrt{T/158,000}$ is small, as

$$\xi = 4.862\,(kT/m_I\,h_I^{\circ})^{1/2}\,[1 - 0.2096\,(kT/m_I\,h_I^{\circ})].$$

Since for hydrogen $m_I\,h_I^{\circ}/k \approx 158,000$ K, then we have

$$k_{LEN} = 1.6 \times 10^{-38}\sqrt{T}\;n_E\,n_N \exp\left[-0.0122\sqrt{T}\,(1 - 5.28 \times 10^{-4}\sqrt{T})\right](cm^{-1})$$

where n_E, n_N are in cm^{-3}.

n_E is given in Eq. (B-1) and the only neutrals present are atoms ($\beta = 1$). Their number density is found the same way to be

$$n_E = 2\,\alpha\,\rho/m_M, \quad n_N = n_A = 2\,(1 - \alpha)\,p/kT\,Z$$

Then the final expression for k_{LEN} is

$$k_{LEN} = \frac{3.33 \times 10^{b}\,\alpha\,(1 - \alpha)\,p^2}{T^{3/2}\,Z^2} \exp\left[-0.0122\sqrt{T}\,(1 - 5.28 \times 10^{4}\sqrt{T})\right]$$

b = -6 for cgs units b = -2 for mks units (B-3)

The expression for k_L to be used in the laser absorption expression, and in the definition of optical depth τ is the sum

$$k_L = k_{LEI} + k_{LEN} \quad . \qquad (B-4)$$

A plot of k_{LEI} (dashed lines) and k_{LEN} (solid lines) is given in Fig. B-1 as k_L/p vs T. It can be seen that electron-ion absorption dominates at temperatures above 11,000 K at 10 atm, above 9,000 K at 1 atm. The sum k_L follows the k_{LEI} curves closely above 12,000 K.

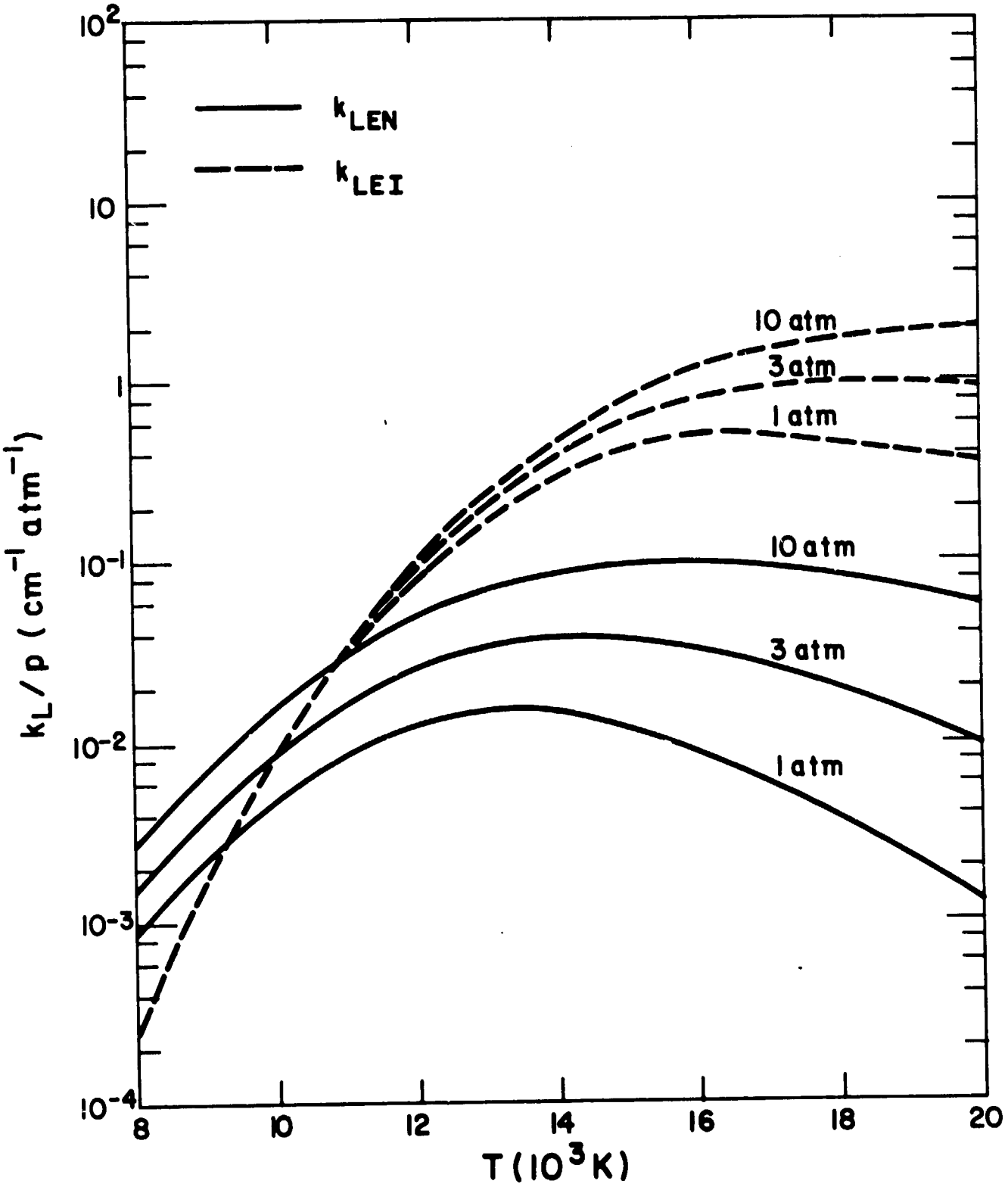

Fig. B-1 Inverse Bremsstrahlung Absorption Coefficient

APPENDIX C

THERMAL CONDUCTIVITY OF HYDROGEN

The only transport property of hydrogen needed is the thermal conductivity. Since we deal with hydrogen in thermal equilibrium we need not only the conductivity due to the motion of the particles, usually called the frozen conductivity, but also that due to the transport of energy of the various species. The total heat flux in a chemically reacting gas, in the x direction, can be written as

$$q = - \lambda_F \frac{\partial T}{\partial x} + \sum \rho_i u_i h_i$$

The first term is the transport of energy relative to the mass average speed, and the second term is the transport of energy with the diffusion velocity of each species, u_i, which is the average velocity of the i-th species with respect to the mass average velocity. The diffusion velocity depends on concentration gradients and temperature gradients. In equilibrium, the concentration gradient also depends on the temperature gradient, so we may write

$$u_i = - D_i \partial T / \partial x \ .$$

Then the heat flux becomes

$$q = - (\lambda_F + \sum \rho_i D_i h_i) \partial T / \partial x \ .$$

The summation term is the contribution caused by the differing average velocity of each species, carrying the enthalpy of that species, and includes changes of concentration due to chemical reactions. The total thermal conductivity is the sum

$$\lambda_C = \lambda_F + \sum \rho_i D_i h_i \ .$$

The calculation of the D_i is quite complicated since it involves the species diffusion coefficients, as well as the changes in local concentration due to reactions. Very little work on this subject has been done for hydrogen. The only work known to the authors which covers the high temperature range is that of Yos, Ref. A6. Yos provides a table of λ_C for hydrogen at pressures of 1, 3, 10 and 30 atm for the temperature range 1000 (1000) 10,000 (2000) 30,000. Since duplication of his calculations would be a difficult task, we have chosen to use his table and interpolate. The appropriate table (Yos' Table III) is reproduced here in MKS units as Table C1.

At each pressure, λ_C has two peaks, one around 4000 to 5000 K, and one around 14000 to 18000 K. The first reflects the effect of dissociation, the second the effect of ionization.

In order to obtain λ_C for intermediate temperatures, at any of the four pressures in the table, a quadratic interpolation scheme was used, with the middle value of T taken nearest to the value of T at which λ_C is desired.

For $T < 1000$, a linear fit was made between 0.437 at 1000 K and 0.177 at 300 K,

$$\lambda_C = 3.71 \times 10^{-4} T + 6.56 \times 10^{-2} \qquad \text{(C-1)}$$

The value 0.177 at 300 K was taken from p. 574 of Ref. A7, which gives an experimental value of 4227 cal/cm-s-K.

For the computation of the thermal conductivity loss due to lateral temperature variation, the integral

TABLE C1

EQUILIBRIUM THERMAL CONDUCTIVITY OF HYDROGEN λ_C (W/mK)

(Yos, Ref. A6, Table III)

T (10^3K)	p (atm)			
	1	3	10	30
1	0.437	0.437	0.437	0.437
2	0.903	0.862	0.837	0.823
3	6.90	4.62	3.12	2.33
4	14.8	15.5	12.3	8.77
5	3.63	6.49	11.1	13.3
6	2.24	2.78	4.40	7.43
7	2.36	2.48	2.90	4.00
8	2.71	2.71	2.82	3.22
9	3.22	3.12	3.10	3.22
10	4.00	3.72	3.57	3.55
12	5.90	5.31	4.88	4.61
14	7.58	7.11	6.51	6.09
16	6.48	7.67	7.83	7.54
18	4.23	6.20	7.87	8.48
20	3.30	4.70	6.81	8.44
22	3.32	4.19	5.85	7.78
24	3.71	4.34	5.60	7.37
26	4.30	4.88	5.90	7.38
28	5.00	5.57	6.49	7.76
30	5.77	6.38	7.33	8.52

$$I_{\lambda_C} = \int_{300}^{T} \lambda_C(T)\, dT$$

is needed. This was obtained at the same temperatures and pressures by a Simpson's rule integration of λ_C, as interpolated in Table C1. The value at 1000 K is the integral of Eq. (C-1):

$$I_{\lambda_C}(1000) = \int_{300}^{T} (3.71 \times 10^{-4}\, T + 6.56 \times 10^{-2})\, dT$$

$$= 3.71 \times 10^{-4} \times .5\, (10^6 - 9 \times 10^4) + 6.56 \times 10^{-2} (1000-300)$$

$$= 215 \text{ W/m}$$

The values so obtained are given in Table C2. At other temperatures, the integral was obtained by the same interpolation scheme as used for λ_C.

TABLE C2

INTEGRAL OF THERMAL CONDUCTIVITY I_{λ_C} (W/m)

T (10^3K)	p (atm)			
	1	3	10	30
1	215	215	215	215
2	424	587	695	752
3	4167	2734	2099	1917
4	16606	14452	10674	7626
5	25006	25005	22832	19528
6	27815	29356	30149	29690
7	30096	31942	33680	35184
8	32618	34522	36510	38729
9	35560	37421	39455	41921
10	39148	40825	42774	45279
12	49084	49820	51170	53369
14	63028	62447	62612	64074
16	77280	77565	77166	77789
18	87770	91440	93049	93972
20	95141	102175	107712	110995
22	101699	110955	120254	127174
24	108696	119420	131612	142254
26	116688	128615	143064	156942
28	125976	139045	155412	172019
30	136718	150947	169127	188139

APPENDIX D

RADIATIVE PROPERTIES OF HYDROGEN

Radiative transfer influences the hot hydrogen plasma in two ways. A portion of the radiation escapes from the plasma and therefore corresponds to an energy loss term in the fluid dynamic equations for the system. In addition, some of the radiation is transported into the cold gas upstream of the LSC wave and is absorbed there. The rate at which this energy transport occurs is a primary factor in controlling the propagation of the LSC wave, since without the initial heating by either radiation or thermal conduction, the hydrogen cannot absorb the laser radiation. In this Appendix we review the modeling of the radial radiative losses which was undertaken in the previous report[A2] and we introduce a model of the forward axial transport which is suggested by our previous modeling of LSC waves[A8] in air.

D1 Radiative Loss From the Bulk Plasma

The radiative losses from the hot hydrogen plasma can be determined from a knowledge of the spectral radiative properties of an element of plasma. For the temperatures and pressures expected in the hot core of a laser-heated rocket engine, that is, temperatures between 10000K and 20000K and pressures between one and ten atmospheres, the plasma is in local thermodynamic equilibrium. The radiative properties are then summarized by the effective spectral absorption coefficient $k'_\omega(T,p)$ which includes the effects of stimulated emission.

The calculation of k'_ω need only include those transitions which make significant contributions to the radiation in the regime of interest. The concentration of hydrogen molecules is negligible in the hot core, hence only

transitions involving atoms, ions or electrons are important. Three distinct types of transitions occur — free-free transitions (bremsstrahlung), free-bound transitions (photo-recombination), and bound-bound transitions (spectral lines). For our purposes, bremsstrahlung and photo-recombination into the excited states can be adequately described by the semi-classical approximation (Kramer's formula).[A9] The quantum mechanical expression for photo-recombination into the ground state is given by Bethe and Salpeter.[A10] The strength of an atomic line is usually expressed by the oscillator strength f. Quantum mechanical calculations of f are used for the dominant lines, and semi-classical formulas for the higher series members. The profile of the lines in the Lyman and Balmer series are important for estimating reabsorption. The asymptotic Holtsmark profile adequately describes the Lyman series lines for this purpose. The exact Stark-broadened profile of Griem[A11] is required for H_α, the first member of the Balmer series. Reabsorption is unimportant for higher members of the Balmer series. A more detailed description of the radiative properties of hydrogen can be found in the previous report, Ref. A2.

A plot of the emission coefficient ϵ_ω for a transparent hydrogen plasma is illustrated in Fig. D1. We have chosen a temperature of 18000K and a pressure of 3 atmospheres, which are conditions typical of the rocket core. The continuum contribution -- bremsstrahlung and photo-recombination -- is given by the cross hatched region, whereas the contribution from spectral lines is hatched with diagonal lines. For reference, the black body function $B_\omega(T)$ divided by 2R (for R = 0.5 cm) is also plotted. The ratio ϵ_ω divided by $B_\omega/2R$ gives $k'_\omega(T, p)$ in cm^{-1}. Examination of Fig. D1 reveals that the bulk of the radiation occurs in the spectral region of ω greater than 8 eV. This radiation is produced by transitions to the ground state. It should also be noted that above 13 eV the spectral line contribution no longer shows distinct lines but rather resembles the continuum. Therefore the continuum for transitions to the bound state effectively extends to photon energies below 13 eV, a fact which is used in the subsequent modeling of axial transport.

C-2

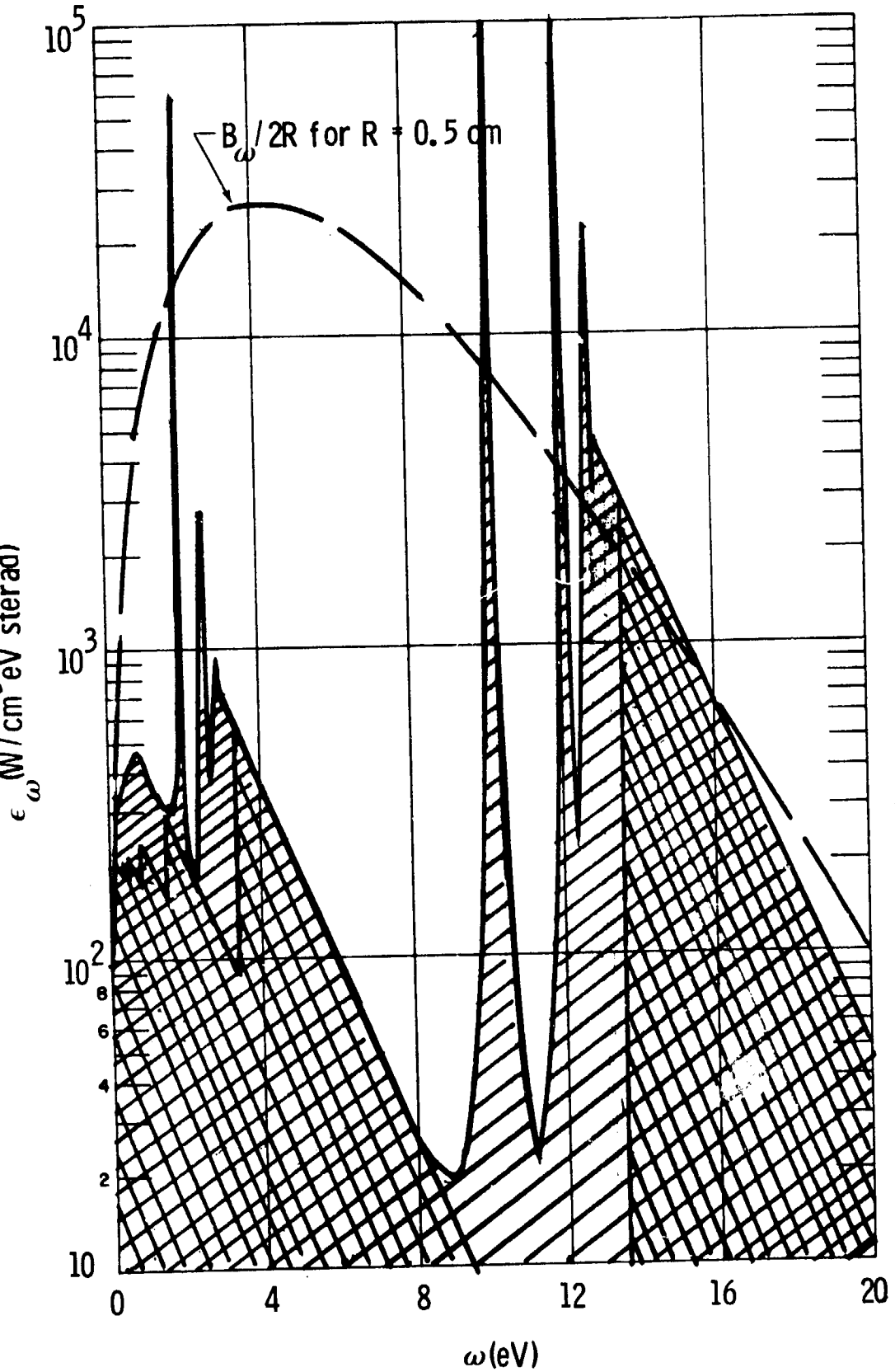

Fig. D1 Transparent emission coefficient for 18,000K, e atm hydrogen. Continuum is cross hatched, lines are hatched with diagonal lines. Blackbody spectral intensity B_ω, divided by 2R for R = 0.5 cm, is shown for comparison.

The emission from the Lyman α line swamps all other radiation in the transparent approximation. It is essential, therefore, to incorporate into the model the effect of reabsorption. The amount of reabsorption depends upon geometry as well as the pressure and temperature distribution. In order to model the bulk radiative loss, the rocket is assigned a characteristic pressure p and a characteristic radius R. (The radiation does not change significantly for the small deviations from p and R which occur within the rocket core.) Then the radiation emitted from an element of plasma at temperature T can be estimated by calculating the average radiation emitted per unit volume from an infinite cylinder of plasma which has radius R, temperature T, and pressure p. The exact solution for the average loss per unit volume for any spectral region can be adequately approximated, for the present scenario, by using the optically thin limit for the emission coefficient per unit volume whenever the criteria $2k'_\omega R \leq 1$ is satisfied, and by using the black body spectral function to describe the radiation per unit surface area whenever $2k'_\omega R \geq 1$ is true. The portions of the spectrum which are extremely black, for example the center of strong lines, should not be considered as a bulk loss. Their radiation is controlled by surface effects and cannot be reliably predicted without information about the radial temperature gradients. Since these gradients are not included in the fluid dynamic formulation, we also neglect radiation which is sensitive to these gradients. In the cases studied, the spectral absorption coefficient corresponds to the plasma being transparent or marginally black ($2k'_\omega R \leq 3$), or else to the plasma being strongly black ($2k'_\omega R \geq 10$). In our estimates of bulk radiative losses, the strongly reabsorbed contribution ($2k'_\omega R \geq 10$) is omitted.

Numerical calculations have been made of the bulk plasma loss versus temperature for a variety of pressures and radii. For insertion into computer codes the numerical predictions can be fitted by an analytic form suggested from an analysis of the semi-classical continuum radiation. The power lost per unit volume P_T, is given by

$$P_T = 8.9 \times 10^{-9} \frac{C_1 T}{\theta_I} \left(\frac{T}{\theta_I} + C_2\right) n_{AG} e^{-\theta_I/T} \left[\frac{W}{cm^3}\right] ,$$

where C_1 and C_2 are constants, θ_I is the ionization potential expressed in degrees K, and n_{AG} is the number density of atoms in the ground state in cm^{-3}. Expressed in terms of the number of atoms, n_A, we have $n_{AG} = 2n_A/Q_{elA}$, where n_A is found from (A-4), (A-7) and (A-14) of Appendix A, and the electronic partition function of the atoms Q_{elA} is given in (A-17). When expressed in MKS units, as used for calculations, we then find

$$P_T = 17.2 \times 10^{-9} \frac{C_3 T}{\theta_I} \left(\frac{T}{\theta_I} + C_2\right) \frac{n_A}{Q_{elA}} e^{-\theta_I/T} \left[\frac{W}{m^3}\right] . \qquad (D-1)$$

The values of the constants C_3 and C_2 appropriate to various cases calculated are given in the table in Subsection 2.3 of the main text.

D2 Axial Radiative Transport

An important component of the propagation mechanism for LSC waves in air is known to be the forward axial transport of radiant energy from the vacuum ultraviolet portion of the spectrum. The same mechanism is expected to be important for LSC waves in hydrogen since the hot hydrogen plasma emits in the VUV much the same as an air plasma does, and the cool hydrogen atoms upstream of the plasma strongly absorb this radiation. We are led, therefore, to model the forward transport in hydrogen in the manner which has proven successful for air LSC waves.[A8]

The first step is to determine the region of the spectrum which contributes to forward transport. For radiation to be an effective transport mechanism, it must be strongly absorbed by the cool gas which cannot absorb the laser radiation, and it must be emitted strongly by hot plasma. Only radiation involving transitions to the ground state atom satisfies both criteria.

Fig. D1 can be used to identify the region further. The continuum effectively begins somewhere between 12eV and 13eV because of the merging of spectral lines. The stronger lines are distinct and should not be included in our estimate of forward radiative transport since these lines tend to become narrower at lower temperature, and therefore, even though the lines are strong emitters, they do not satisfy the criterion that they also be strong absorbers over the same spectral range at low temperature. Morevoer, at lower temperatures, several of the lines which are shown merged in Fig. D1 become distinct, and once again the criteria of strong absorption in the cool gas is no longer satisfied. As a conservative estimate of the portion of the spectrum which contributes to forward radiative transport, we choose the continuum having photon energy $\omega \geq 13.0$eV.

An expression for the absorption coefficient for photoionization of the ground state has been derived by Bethe and Salpeter (Ref. A10, pp 304-5). In the region of interest in the present calculations ($13 < \omega < 26$eV), they give

$$k_\omega \ [cm^{-1}] = 6.34 \times 10^{-18} \left(\frac{\omega_I}{\omega}\right)^{8/3} n_{AG} \ [cm^{-3}] \quad , \qquad (D\text{-}2)$$

where ω_I is the photon energy at the beginning of the true continuum, namely $\omega_I = 13.6$eV. The full expression (D-2) can be used in numerical computations; however, for discussions of the general properties of the VUV radiation, it is convenient to define a single absorption coefficient which is characteristic of the VUV. An appropriate value is

$$(k_{VUV})_A \ [cm^{-1}] \equiv 6.34 \times 10^{-18} \ n_{AG} \ [cm^{-3}] \quad .$$

For the computations performed by the computer, the molecular hydrogen concentration never gets large enough to warrent its inclusion in

the estimate of k_{VUV}. However, in order to justify the assertion that all radiation emitted in the VUV is absorbed in the cool gas, we have computed k_{VUV} for temperatures as low as 2000K. Here absorption by molecular hydrogen dominates. The molecular absorption spectrum is characterized by an ionization continuum for $\omega \geq 15.5$eV, a dissociation continuum for $15.5 \geq \omega \geq 14.8$eV and sharp absorption bands for $\omega \leq 16.8$eV. While it is not easy to associate a single absorption coefficient with the VUV region, $\omega \geq 13.0$eV, we choose a conservative value of

$$\left(k_{VUV}{}_{M}\right)[cm^{-1}] = 5 \times 10^{-18}\, n_M\ [cm^{-3}] \quad ,$$

where n_M is the number density of molecule, in order to estimate the effects of molecular absorption. This value represents half the experimentally observed cross section at $\omega = 17.7$eV, as recorded by Hudson.[A12]

A plot of

$$k_{VUV} = (k_{VUV})_A + (k_{VUV})_M \quad ,$$

is shown in Fig. D2 for pressures of one, three, ten and thirty atmospheres. In order that all four pressures may be plotted on the same graph, the absorption coefficient is divided by the pressure in atmospheres. It can be seen that at temperatures expected in the hot core ($T \sim 18000$K), the mean free path of VUV photons is 4 cm at one atmosphere, 0.6 cm at 3 atm, 0.1 cm at 10 atm and 0.025 cm at 30 atm. Since the hot core does not change temperature appreciably over a mean free path in the hot plasma, the radiation stays near equilibrium with the plasma, and the radiative transport can be approximated by the radiative conduction model that is, the divergence of the VUV flux is given by

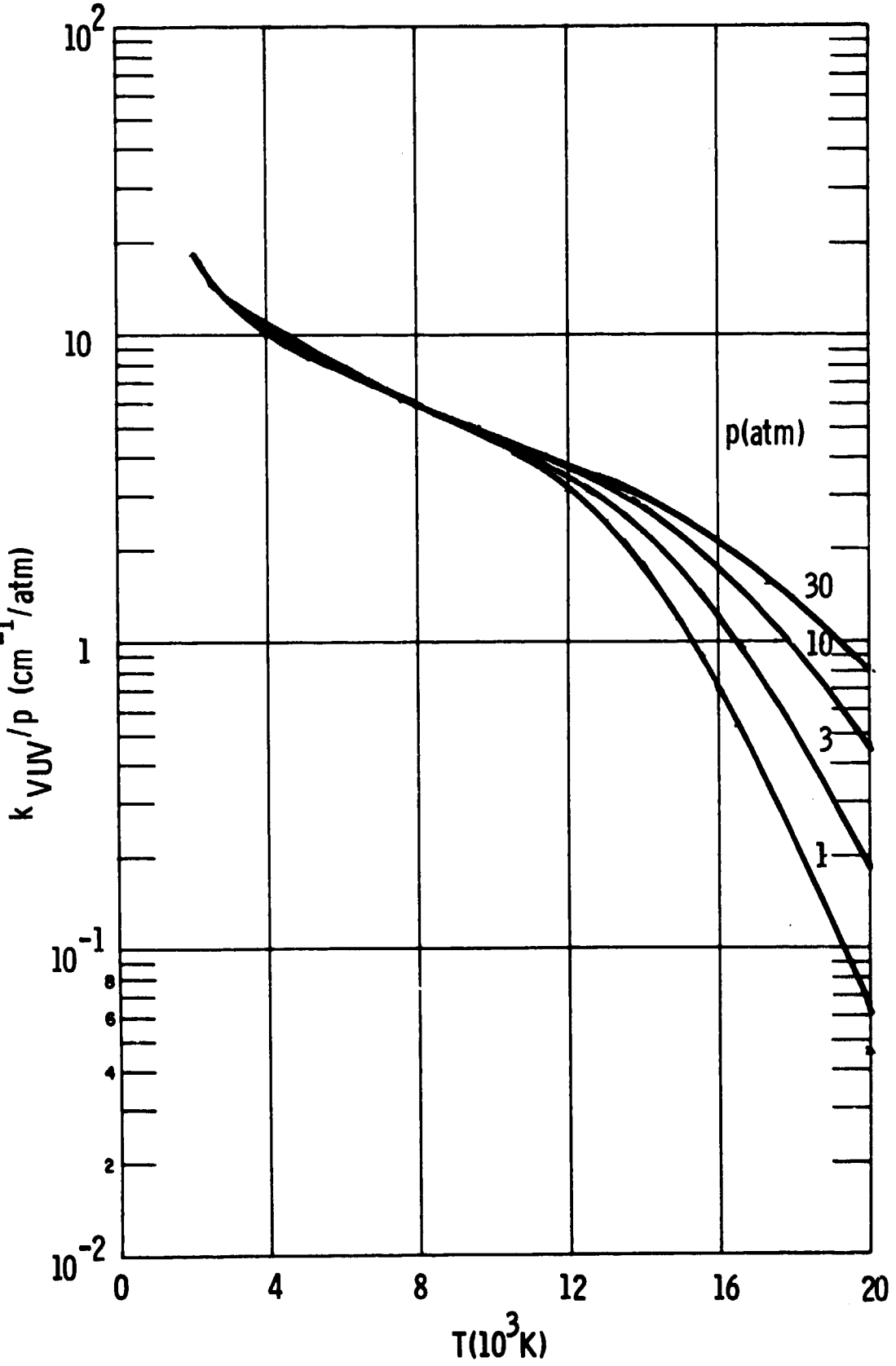

Fig. D2 Absorption coefficient of hydrogen for VUV radiation for 1, 3, 10, 30 atm.

$$\frac{d\,S_{VUV}}{dx} = \frac{d}{dx}\left(\lambda_{VUV}\frac{dT}{dx}\right) \quad , \tag{D-3}$$

where S_{VUV} is the plasma radiative flux in the VUV, and λ_{VUV} is the radiative conductivity defined by

$$\lambda_{VUV} = \frac{4\pi}{3}\int_{VUV}\frac{\partial B_\omega}{\partial T}\frac{d\omega}{k'_\omega} \quad . \tag{D-4}$$

The effective absorption coefficient is found from (D-2) as

$$k'_\omega = (1 - e^{-\omega/kT})\,k_\omega \tag{D-5}$$

where k is the Boltzmann constant. For $\omega \geq 13.0$ eV and T less than 30,000K, the exponential term is negligible. The derivative of the spectral black body function is

$$\frac{\partial B_\omega}{\partial T} = \frac{5,040}{11,605}\,\frac{\omega^4}{T^2}\,\frac{e^{\omega/T}}{(e^{\omega/T}-1)^2}\left[\frac{W}{cm^2\ eV\ K}\right] \quad , \tag{D-6}$$

where T and ω are measured in eV.

When (D-5), (D-2) and (D-6) are inserted into the integral of (D-4), the integration over ω is quite complicated. To simplify it, we change the power in (D-2) from 8/3 to 3, and leave off the factor $(1 - e^{-\omega/T})^3$ in the denominator, of the integral in (D-4), which approximations have counteracting effects. Then the integral is

$$\int_{13}^{\infty} w^7 \exp\left(-\frac{11,605w}{T}\right) dw$$

$$= \frac{7!\, e^{-13 \times 11,605/T}}{(11,605/T)^8} \sum_{\ell=0}^{7} \frac{(13 \times 11,605/T)^{\ell}}{\ell!} \quad ,$$

where T is now in K. With this, we can write (D-4) in MKS units as

$$\lambda_{VUV} = \frac{0.775 \times 10^{30}}{T^2} \frac{Q_{elA}}{n_A} \frac{7!\, e^{-150,865/T}}{(11,605/T)^8} \sum_{\ell=0}^{7} \frac{(150,865/T)^{\ell}}{\ell!} \quad . \quad \text{(D-7)}$$

This is the form used for λ_R in the calculation when the factor given below in (D-8) is appended to account for size effects.

This model suffices for the description of the hot core of a one dimensional wave. At the wave front, however, the temperature changes abruptly. In air LSC waves, the slope of the temperature profile is approximately 2.5×10^4 K/cm at one atmosphere.[A13] The radiation conduction model cannot give reliable predictions of the local radiative properties in the region of the wave since the temperature changes drastically within a photon mean free path. However, since the conduction model does conserve energy, it can give reasonable predictions of quantities, such as wave velocity and core temperature, which depend mainly upon the amount of energy transported forward, but do not depend upon the details of the wave front. Therefore, the radiative conduction model is still applicable provided that the radiation from the hot core is absorbed quickly. This assumption can be justified

by an examination of the optical thickness of the wave front. Assuming a linear temperature profile between T_{min} and T_{max}, the optical depth is given by

$$\tau(T_{max}, T_{min}) = \int_{x(T_{min})}^{x(T_{max})} k'_{VUV}(T)\, dx = \frac{dx}{dT} \int_{T_{min}}^{T_{max}} k'_{VUV}(T)\, dT .$$

A plot of

$$\hat{\tau}(T) \equiv \int_{T}^{20000K} k'_{VUV}(T)\, dT/p$$

for four values of pressures p is shown in Dig. D3. The optical depth between any two temperatures T_{min} and T_{max} can then be computed from $\hat{\tau}$ by evaluating

$$p\left(\hat{\tau}(T_{min}) - \hat{\tau}(T_{max})\right)\Big/\frac{dT}{dx} \qquad \text{(D-8)}$$

The slope of the temperature in the wave front is expected to vary almost linearly with pressure. Based upon the measurements at atmosphere[A13], the maximum slope anticipated in a physical wave is then

$$\frac{dT}{dx} = (2.5 \times 10^4\ p[atm])K/cm \quad .$$

Consider an LSC wave plasma at three atmospheres and 18000K. If the wavefront has the maximum slope, the optical depth between 18000K and 10000K is found from (D-8) and Fig. D3 to be 0.72. Between 18000K and 5000K the optical depth is 2.1. The fraction of the plasma radiation at

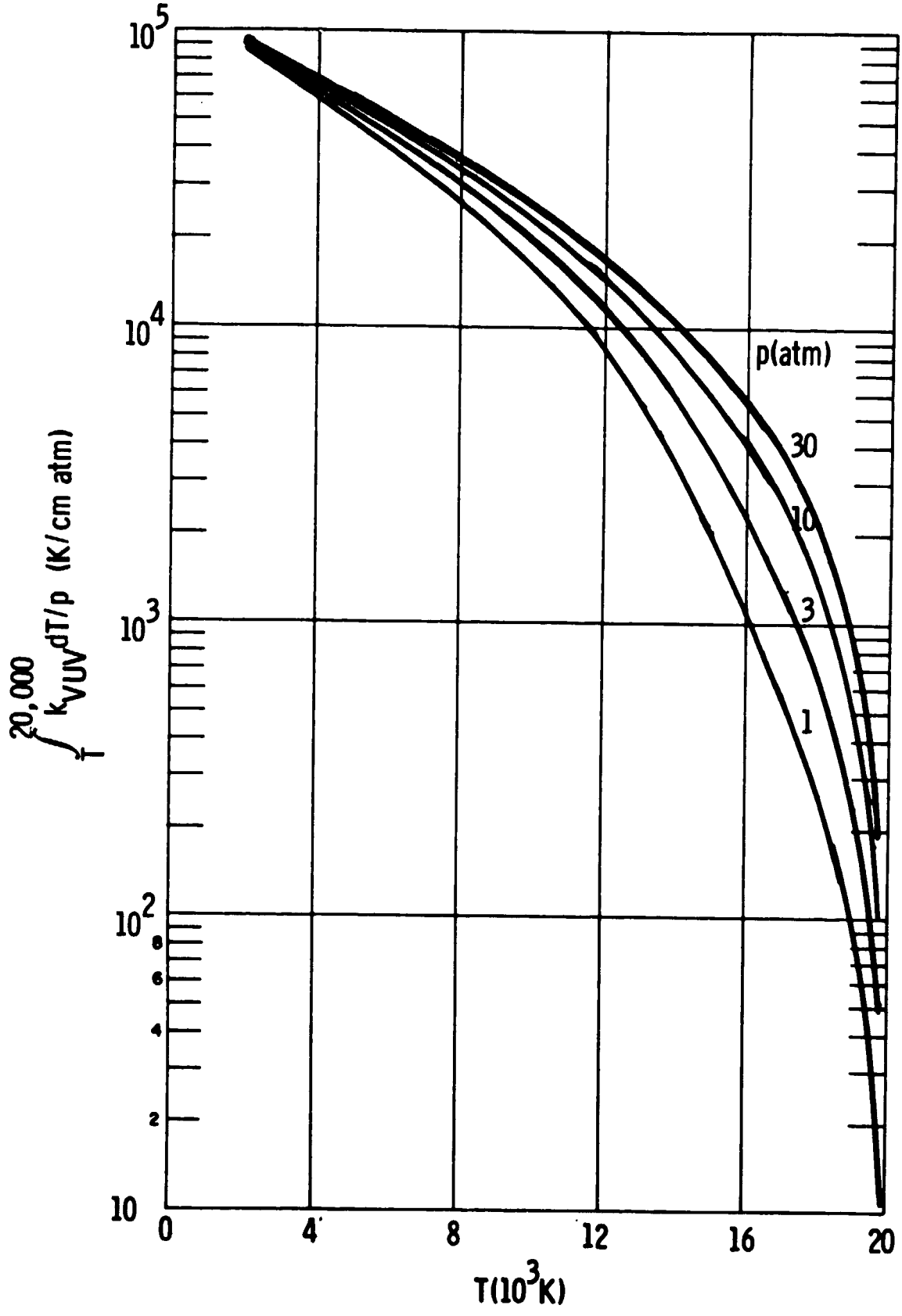

Fig. D3 Integral of effective absorption coefficient of hydrogen for VUV radiation at 1, 3, 10, 30 atm. Optical depth of LSC wave front is proportional to this quantity.

18000K which is absorbed before reaching the place in the wave front where the temperature is 10000K can be conservatively estimated as $1 - e^{00.72} = 0.5$. This is an underestimate because radiation from the hot plasma which is not parallel to the axis is absorbed at a faster rate. Similarly we find 0.88 of the plasma radiation is absorbed by the point where the temperature falls to 5000K. It is reasonable, therefore, to model the forward VUV radiation as being totally absorbed and to use the radiative conduction model to describe forward radiative transport in the VUV.

D3 Finite Radius Considerations

The calculation of bulk losses from the hot plasma includes the effect of radius in the reabsorption effects. Only radiation which was transparent or marginally black ($2k'_\omega R \leq 3$) is included in these estimates. The radiation which is strongly black is omitted since it is associated with radial gradients. However, for calculations made with a radial conduction loss term, as described in Subsection 4.1, it is possible to include VUV radial losses whenever they are not included in the bulk loss term. For the 10 kW and 5 MW devices, the value of C_2 in (D-1) is related to the reabsorption of VUV – a value of 2.4 corresponds to the inclusion of VUV, whereas a value of 0.4 corresponds to the omission of VUV radial radiation. In the latter case, the radiative conduction model can be used to estimate radial losses in the VUV by inserting the total thermal conductivity $\lambda_C + \lambda_{VUV}$ into the model for radial conduction losses. Of course this modification should be made only for the large device – the small device already has the radial VUV losses included.

The finite radius also affects the forward axial transport. If the radius is much larger than the mean free path of the VUV photons, it is appropriate to use the one dimensional model for forward transport. However, if the radius is small compared to the mean free path of the VUV photon, the forward axial flux is severly limited by geometrical considerations. For

example, the axial flux S at the center of the end of a semi infinite cylinder of radius R, as shown in Fig. D4, is given by

$$S = \pi B_\omega(T) \left[1-2E_3 (k'_\omega R)\right] \quad ,$$

where $B_\omega(T)$ is the spectral black body function, k'_ω is the effective spectral absorption coefficient, R is the radius, and E_3 the exponential integral

$$E_3 (y) \equiv \int_1^\infty \frac{e^{-yx}}{x^3} dx \quad .$$

(It is interesting to recall that the same relationship between flux and optical depth $k'_\omega R$ holds for planar slabs of thickness R.)

In the spirit of the approximations made in the determination of radial losses, the black - transparent approximation is also used to include the geometrical effect for forward axial transport; that is, whenever $2k'_\omega R \leq 1$ is true the flux is given by the transparent approximation $2\pi B_\omega k'_\omega R$, whereas whenever the black criteria $2k'_\omega R \geq 1$ holds, the usual black body flux πB_ω is used. This modification affects the radiative thermal conductivity λ_R used to model axial transport in the following way:

$$\lambda_R = \lambda_{VUV} \times \left\{ \begin{matrix} \text{the smaller of} \\ 1 \text{ or } 2Rk'_{VUV} \end{matrix} \right\} \qquad \text{(D-9)}$$

This modified formula has been employed in the calculations discussed in the text. It is to be used only for calculations of axial transport – the radial loss term mentioned above uses the unaltered λ_{VUV}.

Fig. D4 The flux S through the center of the end of a semi-infinite cylinder of radius R.

In the calculation of the radial losses, the integral of $\lambda_R = \lambda_{VUV}$ with respect to temperature

$$I_{\lambda_R} = \int_{300}^{T} \lambda_R \, dT \quad ,$$

is needed. This was obtained at p = 1, 3, 10, 30 atm by a Simpson's rule integration. The results are shown in Table D1. At other temperatures, the value was found by quadratic interpolation.

TABLE D1

INTEGRAL OF RADIATION CONDUCTIVITY I_{λ_R} (W/m)

$T(10^3 K)$	p(atm)			
	1	3	10	30
1	0	0	0	0
2	0	0	0	0
3	0	0	0	0
4	0	0	0	0
5	0	0	0	0
6	4.14E-3	1.39E-3	4.3E-4	1.57E-4
7	2.12E-1	7.07E-2	2.14E-2	7.33E-3
8	4.27	1.42	4.28E-1	1.44E-1
9	4.62E1	1.53E1	4.60	1.54
10	3.25E2	1.07E2	3.19E1	1.06E1
12	7.10E3	2.23E3	6.47E2	2.12E2
14	8.69E4	2.41E4	6.47E3	2.03E3
16	8.81E5	1.94E5	4.44E4	1.28E4
18	8.39E6	1.41E6	2.54E5	6.42E4
20	6.87E7	9.50E6	1.35E6	2.84E5
22	4.49E8	5.63E7	6.69E6	1.18E6
24	2.35E9	2.81E8	3.00E7	4.58E6
26	1.01E10	1.18E9	1.20E8	1.65E7
28	2.89E10	4.32E9	4.23E8	5.47E7
30	5.94E10	1.39E10	1.33E9	1.65E8

APPENDIX REFERENCES

A1. Mayer, J. E. and Mayer, M. G., "Statistical Mechanics," John Wiley and Sons, Inc., New York, 1940.

A2. Kemp, N. H., Root, R. G., Wu, P. K. S., Caledonia, G. E. and Pirri, A. N., "Laser-Heated Rocket Studies," NASA CR-135127 (PSI TR-53), Physical Sciences Inc., Woburn, MA, May 1976.

A3. Zeldovich, Ya. B. and Raizer, Yu. P., "Physics of Shock Waves and High-Temperature Hydrodynamic Phenomena," Ed. by Hayes and Probstein, Academic Press, New York, 1966.

A4. Patch, R. W., "Absorption Coefficients for Hydrogen: I, Composition," J. Quant. Spectroscopy and Radiative Transfer, Vol. 9, 1969 pp. 63-87. Patch, R. W., "Thermodynamic Properties and Theoretical Rocket Performance of Hydrogen to 100,000 K and 1.01325 X 10^8 N/m^2," NASA SP-3069, 1971.

A5. Caledonia, G. E., Wu, P. K. S., and Pirri, A. N., "Radiant Energy Absorption Studies for Laser Propulsion," NASA CR-134809 (PSI TR-20), Physical Sciences Inc., Woburn, MA, March 1975.

A6. Yos, J. M., "Transport Properties of Nitrogen, Hydrogen, Oxygen and Air to 30,000 K," RAD-TM-63-7, Avco Corporation, Wilmington, MA, March 1963.

A7. Hirshfelder, J. O., Curtiss, C. F., and Bird, R. B., "Molecular Theory of Gases and Liquids," John Wiley and Sons, Inc., New York, Corrected Printing with Notes Added, 1964.

A8. Pirri, A. N., Kemp, N. H., Root, R. G. and Wu, P. K. S., "Theoretical Laser Effects Study", Final Report to Naval Research Laboratory on Contracts N00014-74-C-0207 and N00173-76-C-0216 (PSI TR-89), Physical Sciences Inc., Woburn, MA.

A9. Zeldovich, Ya. B. and Raizer, Yu. P., "Physics of Shock Waves and High Temperature Hydrodynamic Phenomena", Vol. I, Academic Press, New York, 1966, p. 265.

A10. Bethe, H. A. and Salpeter, E. E., "Quantum Mechanics of One- and Two-Electron Atoms", Springer-Verlag, Berlin, 1957, p. 265.

A11. Griem, H. R., "Plasma Spectroscopy", McGraw-Hill, New York, 1964, pp. 445 - 448. Also Griem, H. R., "Spectral Line Broadening by Plasmas", Academic Press, New York, 1974, p. 313.

A12. Hudson, R. D., "Critical Review of Ultraviolet Photoabsorption Cross Sections for Molecules of Astrophysical and Aeronomic Interest", Reviews of Geophysics and Space Physics, Vol. 9, No. 2, May 1971, pp. 358 - 360. Also NSRDS-NBS 38, National Bureau of Standards, Washington, DC, August 1971, pp. 54 - 56.

A13. Klosterman, E. L. and Byron, S. R., "Measurement of Subsonic Laser Absorption Wave Propagation Characteristics at 10.6 μm," Journal of Applied Physics, Vol. 45, No. 11, November 1974, pp. 4751 - 4759. Also Fowler, M. C. and Smith, D. C., "Ignition and Maintenance of Subsonic Plasma Waves in Atmospheric Pressure Air by CW CO_2 Laser Radiation and Their Effect on Laser Beam Propagation", Journal of Applied Physics, Vol. 46, No. 1, January 1975, pp. 133 - 150.